

# The Host Galaxies of High Velocity Type Ia Supernovae

Anya E. Nugent<sup>1</sup>, Abigail E. Polin<sup>2,3</sup>, and Peter E. Nugent<sup>4</sup>

<sup>1</sup> Center for Interdisciplinary Exploration and Research in Astrophysics (CIERA) and Department of Physics and Astronomy, Northwestern University, Evanston, IL 60208, USA

e-mail: [anyanugent2023@u.northwestern.edu](mailto:anyanugent2023@u.northwestern.edu)

<sup>2</sup> Carnegie Observatories, 813 Santa Barbara Street, Pasadena, CA 91101, USA

<sup>3</sup> TAPIR, Walter Burke Institute for Theoretical Physics, 350-17, Caltech, Pasadena, CA 91125, USA

<sup>4</sup> Lawrence Berkeley National Lab, 1 Cyclotron Road, Berkeley, CA 94720, USA

May 9, 2024

## ABSTRACT

In recent years, there has been ample evidence that Type Ia supernova (SNe Ia) with high Si 2 velocities near peak brightness are distinguished from SNe Ia of lower velocities and may indeed represent a separate progenitor system. These SNe Ia can contaminate the population of normal events used for cosmological analyses, creating unwanted biases in the final analyses. Given that many current and future surveys using SNe Ia as cosmological probes will not have the resources to take a spectrum of all the events, likely only getting host redshifts long after the SNe Ia have faded, we need to turn to methods that could separate these populations based purely on photometry or host properties. Here, we present a study of a sample of well observed, nearby SNe Ia and their hosts to determine if there are significant enough differences between these populations that can be discerned only from the stellar population properties of their hosts. Our results indicate that the global host properties, including star formation, stellar mass, stellar population age, and dust attenuation, of high velocity SNe Ia do not differ significantly from those of lower velocities. However, we do find that high velocity SNe Ia are more concentrated toward the center of their hosts, suggesting that their local environments may indeed differ. Future work requires strengthening photometric probes of high velocity SNe Ia and their local environments to distinguish these events and determine if they originate from a separate progenitor.

**Key words.** type Ia supernovae, galaxies, white dwarfs

## 1. Introduction

Type Ia supernovae (SNe Ia) are well-characterized as standardized candles given how their their peak luminosities, colors, and light curves relate to distance, and have thus been powerful tools in determining the expansion rate of the Universe (Riess et al. 1998; Perlmutter et al. 1999). However, the reasoning behind the variations in their light curves and luminosities, which affects our precision on cosmology, remains largely unknown, posing a dilemma in determining how best to and which SNe Ia can be standardized. Currently, all cosmology measurements using SNe Ia are limited by systematic, not statistical, uncertainties (Smith et al. 2020).

One current predicament in SNe Ia cosmology is understanding if SNe Ia with high Si 2 velocities at  $\sim 6150\text{\AA}$  ( $\gtrsim 12,000 \text{ km s}^{-1}$ , measured at the time of peak brightness) can be used alongside lower velocity SNe in cosmology measurements. Several key differences between high and lower velocity SNe Ia have been discussed extensively in the literature. Notably, the high velocity SNe Ia sample appears have a much narrower distribution of expected  $M_B$  versus Si 2 velocities than the lower velocity SNe sample and redder  $B-V$  colors (Wang et al. 2009; Foley & Kasen 2011; Polin et al. 2019). Recent work has suggested that multiple progenitor systems may account for differences in observed luminosities and light curves (Bulla et al. 2020) of SNe Ia, which would complicate the systematics in their use as a preci-

sion tool for cosmology. For example, it has often been proposed that SNe Ia derive from the thermonuclear explosion of a white dwarf that approaches the Chandrasekhar mass limit (see Maoz et al. 2014 for a review). However, there exists both observational and theoretical evidence that many SNe Ia derive from multiple progenitor channels. These include hydrogen-rich SNe Ia-CSM (Dilday et al. 2012; Harris et al. 2018), super-Chandrasekhar (Howell et al. 2006; Hsiao et al. 2020) and sub-Chandrasekhar (sub- $M_{\text{ch}}$ ; Scalzo et al. 2014; Goldstein & Kasen 2018; Shen et al. 2018; Polin et al. 2019; Liu et al. 2023; Ni et al. 2023) mass explosions. Indeed, Polin et al. (2019) found that high velocity SNe Ia likely derive from sub- $M_{\text{ch}}$  explosions, which naturally produce intrinsically redder SNe. However, alternate theories on the origins of high velocity SNe Ia suggest that their host galaxies' global and local environmental properties are the true cause of their observed difference and simply need a different total to selective extinction ratio,  $R_V$ , to be properly standardized. Wang et al. (2009), for example, claims that their redder colors are likely due to local, dustier environments, and Wang et al. (2013) showed they do indeed occur in denser and brighter regions of their hosts. In contrast, Foley & Kasen (2011) proposes that the redder color is an intrinsic color difference. Since several current and many future surveys using SNe Ia for cosmological measurements will be limited to purely photometric data (Vincenzi et al. 2023), it is crucial to consider if the host galaxy properties of these SNe Ia can be used to separate these sub-types

and, more conclusively determine if the differences between these normal and high velocity populations are intrinsic to the progenitor or related to the local environment.

Previous host galaxy analysis of SNe Ia have been instrumental in both progenitor channel studies as well as providing corrections to the observed luminosities of these events for cosmology. The association of SNe Ia with a diverse set of host environments, ranging from star forming to quiescent and low to high mass galaxies, has more conclusively secured their older stellar progenitor origins with a breadth of delay times. The “mass-step” predicament, wherein SNe Ia in higher mass galaxies ( $\geq 10^{10}M_{\odot}$ ) are observed to be more luminous than those in lower mass galaxies, furthermore has led to debates on whether properties of the host galaxy or the SNe Ia progenitor affect the peak luminosity of such events (Kelly et al. 2010; Sullivan et al. 2010; Gupta et al. 2011; Childress et al. 2013). Several studies, for instance, claim that the dust relations in higher mass galaxies cause the observed difference and thus the extinction corrections to SNe Ia in higher mass galaxies should also be different in order for these SNe to be properly standardized (Salim et al. 2018; Brout & Scolnic 2021; Meldorf et al. 2023). Relations between the width of the SNe light curve and host galaxy stellar population age, gas-phase metallicity, and local and total star formation rates (SFR), have also been observed, implying that age of the progenitor might be linked to SNe observables (Sullivan et al. 2006; Neill et al. 2009; Sullivan et al. 2010; Lampeitl et al. 2010; D’Andrea et al. 2011; Gupta et al. 2011; Childress et al. 2013; Pan et al. 2014; Rigault et al. 2020). Thus, a uniform host galaxy comparison between high and low velocity SNe Ia is crucial to inform: (i) if the redness observed in high velocity SNe Ia is due to the host environment or the progenitor; (ii) if the high velocity SN Ia progenitor traces different stellar population properties (e.g. age, mass, star formation, etc.) than lower velocity SNe Ia; and (iii) if global host galaxy properties can be used to separate these sub-classes.

Here, we model and determine the host galaxy stellar population properties of 74 Type Ia SNe, 14 of which are high velocity SNe Ia, 56 of which are low velocity SNe Ia, and 4 of which are SN 1991bg-like (Filippenko et al. 1992). By comparing the host samples and providing uniform stellar population modeling of these categories of SNe Ia, we infer if the redder colors of high velocity SNe Ia and their observable differences from low-velocity SNe Ia can be explained by any host galaxy property. In Section 2, we describe the SNe Ia sample and how they were selected for this study. We detail our archival photometry search for the hosts of the 74 SNe Ia and the stellar population models used for this analysis in Section 3. We discuss our comparisons of host stellar population properties between the several SNe classifications in Section 4. We discuss possible differences in the local environments of these SNe using their offsets from their host center and Na I D equivalent widths in Section 5. We comment on possible separate progenitor systems in Section 6. Finally, our conclusions are in Section 7.

Unless otherwise stated, all observations are reported in the AB magnitude system and have been corrected for Galactic extinction in the direction of the SN (Cardelli et al. 1989; Schlafly & Finkbeiner 2011). We employ a standard WMAP9 cosmology of  $H_0 = 69.6 \text{ km s}^{-1} \text{ Mpc}^{-1}$ ,  $\Omega_M =$

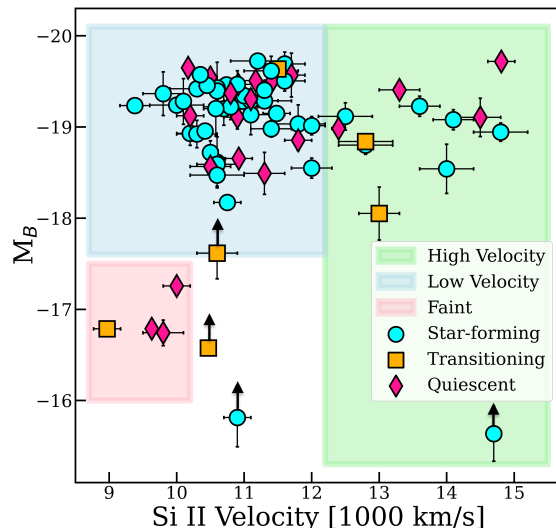


**Fig. 1.** The peak  $B$ -band absolute magnitudes ( $M_B$ ) vs Si 2 velocities with the uncertainties of 74 SNe from the Zheng et al. (2017) and Polin et al. (2021) samples. The SNe are colored by their hosts’ star formation classification: star-forming (blue circles), transitioning (yellow squares) and quiescent (red diamonds). High velocity SNe Ia ( $\geq 12,200 \text{ km/s}$ ) are outlined in the green box, low velocity SNe Ia in the blue box, and SN 1991bg-like faint SNe ( $M_B > -17.5 \text{ mag}$ ) are highlighted in the pink box. Arrows represent SNe Ia that are not intrinsically faint, but rather fainter from some extinction. The entire population is dominated by star-forming galaxies (64%), and the high and low velocity SNe Ia roughly follow those fractions (57% and 70%, respectively).

0.286,  $\Omega_{\text{vac}} = 0.714$  (Hinshaw et al. 2013; Bennett et al. 2014).

## 2. Supernovae Sample

We conduct our host galaxy analysis based on the SNe Ia sample described in Zheng et al. (2017) and Zheng et al. (2018). This sample includes SNe discovered and observed by the Lick Observatory Supernovae Search (LOSS; Filippenko et al. 2001; Leaman et al. 2011), the Harvard Smithsonian Center for Astrophysics Data Release 3 (Hicken et al. 2009), and the Carnegie Supernova Project (Contreras et al. 2010). We note that these surveys are galaxy-targeted and can be constructed to be volume-limited. Their main advantage over other surveys is that they are able to detect faint SNe Ia several magnitudes below peak brightness, and thus can find SNe Ia that have a much smaller contrast with their hosts and/or suffer from local extinction. As the goal of this work is to better understand if faintness and redness in SNe Ia is correlated with host galaxy properties, this sample is preferred over the Palomar Transient Factory (PTF), Zwicky Transient Facility (ZTF), and other magnitude-limited surveys, which are naturally biased against detecting faint SNe or those with low contrast over their host (Frohmaier et al. 2017). These SNe were selected based on the conditions outlined in Zheng et al. (2017), which required SN discovery at 1 magnitude fainter in  $B$ -band than peak brightness and good photometric cov-

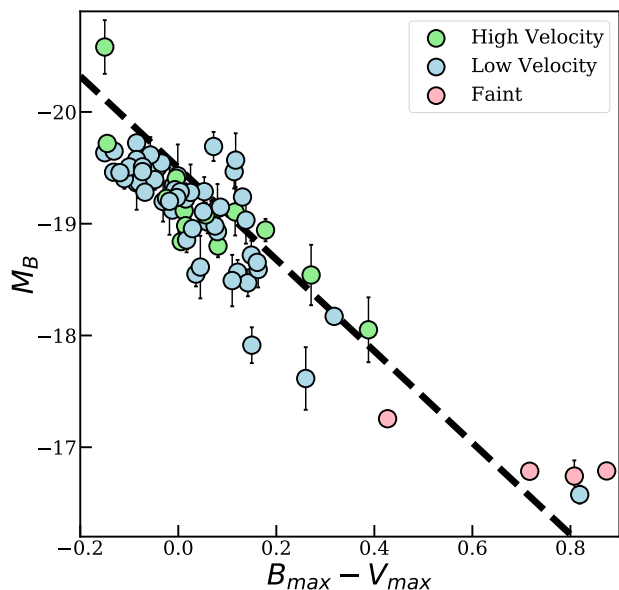


**Fig. 2.** The peak  $B$ -band absolute magnitudes and  $B - V$  colors for high velocity (green), low velocity (blue), and faint SNe Ia (pink). The dashed black line shows the standard Milky Way dust extinction law with  $R_B = 4.1$  and the  $M_B$  intercept represents the  $M_B$  that  $B - V = 0$  for unextinguished SNe Ia in the SNooPy algorithm (Burns et al. 2011). Given that most SNe Ia are extinguished, we do expect that the majority of SNe Ia in our sample will fall below this relation. High velocity SNe Ia trend towards redder colors than low velocity SNe Ia.

erage post-discovery to properly model their lightcurves and estimate their peak luminosities. We include 53 out of the 56 total SNe in this sample based on the available SNe and host galaxy data. The three SNe not used in our analysis did not have sufficient host galaxy photometry for stellar population modeling (see Section 3.1). We additionally include 21 more SNe in Polin et al. (2021) and references therein that have public data in the Weizmann Interactive Supernova Data Repository (WiSeREP; Yaron & Gal-Yam 2012) and the Open Supernovae Catalog (OSC; Guillochon et al. 2017). These SNe Ia have a peak spectrum for Si II velocity measurements, and peak  $B$ -band magnitudes and  $B - V$  colors, thus have comparable data to the Zheng et al. (2017) sample, as well as sufficient host galaxy observations for stellar population modeling. All SNe Ia have spectroscopically confirmed redshifts that range between  $0.0008 < z < 0.04$ . In Table A.1, we present all SN properties used in this work. For each SN, the  $B - V$  values and Si II velocity measurements are obtained from Zheng et al. (2018) and Polin et al. (2021). We correct the  $B$ -band absolute magnitudes in Zheng et al. (2018) and Polin et al. (2021) using the Hubble Flow distance moduli for each SN host acquired from the NASA/IPAC Extragalactic Database (NED). For the majority of SN sample, we use distance moduli from Mould et al. 2000 (“Virgo + GA + Shapely” on NED) and for several others we use the values cited in Saha et al. (2001); Macri et al. (2001); Blakeslee et al. (2010); Riess et al. (2022). We choose these values for consistency across sample and because these distance moduli are corrected most for peculiar velocities.

We divide the SNe sample into several categories based on the extinction-corrected peak  $B$ -band absolute magnitudes ( $M_B$ ) and the Si 2 velocities determined in Zheng et al. (2018): high velocity SNe Ia (Si 2 velocities  $> 12,200 \text{ km s}^{-1}$ ), low velocity SNe Ia ( $< 12,200 \text{ km s}^{-1}$ ), and faint 1991bg-like (Filippenko et al. 1992) SNe ( $M_B > -17.5 \text{ mag}$ ), which we highlight in Figure 1. We classify three SNe that have  $M_B > -17.5 \text{ mag}$  as low velocity rather than faint SNe Ia, as they have positive Na I D equivalent widths at four times the uncertainty at minimum, in contrast to the other faint SNe Ia, (see Section 5.2, Table A.1). This likely implies that they are not intrinsically faint, but rather fainter due to some extinction. Given these sample divisions, we find that 19% of the sample are high velocity SNe Ia, 76% are low velocity SNe Ia, and 5% are faint SNe. We note that only  $\approx 2$  SNe overlap between high and low velocity SNe Ia samples given the uncertainties on the Si 2 velocities. As is shown in Figures 1 and 2, the high velocity SNe Ia appear to have a much narrower distribution of  $M_B$  and Si 2 velocities than low velocity SNe Ia, with lower  $M_B$ , and redder colors. However, we note that choice of these sub-classes is not simply made from random cuts in  $M_B$  and velocity space, as model-independent, statistical methods for dividing the SNe Ia sample has proven these sub-classes are clearly distinguished. For example, using a hierarchical cluster analysis, Benetti et al. (2005) observed a clear population difference between these three categories of SNe using ratios of the Si 2 lines. Burrow et al. (2020) further found these groups of SNe are distinguished between multiple photometric and spectroscopic properties of the SNe using Gaussian mixture models. As there is significant evidence that these SN sub-classes are separate and robust, we focus on the SN host environments to determine if we can use these properties to separate the SN classes and if they point to different progenitor or environmental differences that affect the SN observables, as has been suggested previously (Wang et al. 2009; Foley & Kasen 2011; Wang et al. 2013; Polin et al. 2019; Pan 2020; Pan et al. 2022).

### 3. Host Galaxy Observations & SED Modeling

#### 3.1. Archival Data Collection

We determine host galaxies for each SN through querying nearby ( $\lesssim 5'$ ) galaxies at approximately the same redshift as the SN via the NED. To model the host galaxies' stellar population properties, we require broadband photometric observations in at least three different photometric filters covering at least two wavelength ranges (UV, optical, IR, and mid-IR), ensuring that the spectral energy distribution (SED) is well sampled. We collect archival photometric observations for all host galaxies via NED. We obtain UV, IR, and mid-IR observations through the *GALEX* (Bouquin et al. 2018), Two-Micron All Sky Survey (2MASS) (Skrutskie et al. 2006), and Wide-field Infrared Survey Explorer (WISE; Wright et al. 2010) surveys, respectively. Optical data is from the Sloan Digital Sky Survey (SDSS; *ugriz*; Ahumada et al. 2020) survey and *UBVRI* data available on NED. To mitigate inconsistencies in the photometry selected for the study, we select photometry based on extended source models or wide aperture sizes that, in theory, will encapsulate the majority of the each host's flux. For *GALEX* observations, we use the Kron galaxy photometry if it is available or the elliptical aperture photometry.

For SDSS data, we use the elliptical “Model” photometry as this is optimal galaxies. For 2MASS and WISE data, we use the profile-fit photometry for extended sources or, if that is not available, the photometry with the widest aperture size (ensuring that the same aperture size is used for each survey). We do not use any photometric data that is contaminated by foreground sources. We correct all photometry for Galactic extinction in the directions of the SNe (Cardelli et al. 1989; Schlafly & Finkbeiner 2011). Finally, we require impose a 10% error floor, forcing all uncertainties to be  $\gtrsim 10\%$  the flux density value, to ensure that no photometric observation is overweighted in the stellar population modeling and to mitigate systematic errors that may arise with large aperture photometry. We show all host galaxy photometry in Table B.1.

### 3.2. Stellar Population Modeling

To determine the stellar population properties of the SNe host galaxies, we use the stellar population modeling code *Prospector* (Leja et al. 2017; Johnson et al. 2021). We fit the observational data with *Prospector* through a nested sampling fitting routine, *dynesty* (Speagle 2020), to return posterior distributions of the stellar population properties of interest. *Prospector* produces model SEDs with FSPS (Flexible Stellar Population Synthesis; Conroy et al. 2009; Conroy & Gunn 2010) using single stellar models through MIST (Paxton et al. 2018) and the MILES spectral library (Falcón-Barroso et al. 2011). The main fitted parameters are the age of the galaxy at the time of observation (the maximum allowed value is the age of the universe at the SN’s redshift), total mass formed, stellar metallicity ( $Z_*$ ), and  $V$ -band optical depth.

For all *Prospector* fits, we use the Chabrier (2003) initial mass function (IMF) and a parametric delayed- $\tau$  star formation history (SFH  $\propto te^{-t/\tau}$ ), defined by the  $e$ -folding time  $\tau$ , a sampled parameter. We include the effects nebular emission (Byler et al. 2017) and fix the gas phase metallicity ( $Z_{\text{gas}}$ ) to solar since we do not use an observed spectrum in the modeling and therefore cannot measure spectral line strengths. We constrain the total mass formed and stellar metallicities through the Gallazzi et al. (2005) mass-metallicity relation to probe realistic masses ranges for a given stellar metallicity. We measure dust attenuation through the Kriek & Conroy (2013) model, which includes a sampled parameter that determines the offset from the Calzetti et al. (2000) attenuation curve. Additionally, we allow the fraction of dust attenuated from young to that from old stellar light to be a sampled parameter to create more flexibility in determining the  $V$ -band optical depth, which hereafter we report as a  $V$ -band magnitude ( $A_V$ ). As the majority of hosts have available 2MASS and WISE data, we include the Draine & Li (2007) IR dust emission model, a three-component dust emission model. To balance dimensionality in the model with the available photometry and ensure that that the model is not overfitting the data, we only sample one of the three components: the polycyclic aromatic hydrocarbon mass fraction ( $q_{\text{pah}}$ ). We follow the methods in Nugent et al. (2020) to calculate the stellar mass ( $M_*$ ), present-day star formation rate (SFR), and mass-weighted age ( $t_m$ ) for each host.

Finally, to classify each host by the degree of star formation, we use the definitions in Tacchella et al. (2022), which

measures the combination of the specific SFR (sSFR = SFR/ $M_*$ ; yr $^{-1}$ ) and the Hubble time  $t_H(z)$  at the SN’s redshift:  $\mathcal{D}(z) = \text{sSFR} \times t_H(z)$ . If  $\mathcal{D}(z) > 1/3$ , the host is classified as actively star-forming, if  $\mathcal{D}(z) < 1/20$  the host is quiescent (no active star formation), and if  $1/20 > \mathcal{D}(z) > 1/3$ , the host is transitioning from star forming to quiescent. We describe our main results from stellar population fitting in the following section.

## 4. Global Stellar Population Properties

Here, we discuss the results from the *Prospector* fitting of 74 SNe hosts. In Table 1, we list the median and the 16<sup>th</sup>-84<sup>th</sup> percentile region for the stellar population age, stellar mass, SFR, specific SFR, stellar metallicity, and  $A_V$  for the different types of Ia SNe explored in this paper. We show representative model SEDs in comparison to the selected observed photometry for a high (SN 2004dt) and a low (SN 1999dq) velocity SNe Ia in Figure 3 to highlight the accuracy of our *Prospector* stellar population modeling techniques. We discuss correlations between the *Prospector*-derived stellar population properties in the following subsections. Individual host properties are shown in Table C.1.

### 4.1. Redshift

We first focus on the redshift distributions of the three SNe Ia sub-classes to determine if there are any differences that may bias any of the conclusions in this work, as several stellar population properties (such as age, stellar mass, and SFR) are known to be correlated with redshift. We list the redshift median and the 16<sup>th</sup>-84<sup>th</sup> percentile regions for the three sub-classes in Table 1. We compare the distributions through an Anderson Darling (AD test), with the null hypothesis that the hosts are all derived from the same redshift distribution. If the AD test returns a probability  $P_{AD} < 0.05$ , we can reject the null hypothesis. We list the results of the AD test in Table 2. We find no evidence that high and low-velocity SNe Ia have different redshift distributions. We do, however, find that the the slightly lower median of the faint SNe Ia does result in a rejection of the null hypothesis between high velocity and faint SNe Ia, but not between low-velocity and faint SNe Ia. Given that the majority of our analysis is between high and low velocity SNe Ia, our AD tests show that there will be no redshift-bias on the stellar population properties for these sub-classes.

### 4.2. Star Formation

We next focus on the global star formation properties of the host galaxies to determine if the SN type is related to star formation activity. We highlight the SNe categories with respect to their peak  $M_B$  and Si2 velocities along with their hosts’ star formation classification in Figure 1. We find that 64% of the entire SNe host population are star-forming galaxies, with 28% quiescent galaxies, and 8% transitioning. This roughly follows the star-forming fraction of the observed Type Ia SNe host population (Mannucci et al. 2008). We list the star-forming, transitioning, and quiescent fraction for the three SNe Ia sub-classes in Table 1. The high and low velocity SNe Ia hosts roughly follow the fractions of the entire population and the faint SNe hosts are dominated by quiescent galaxies. To test whether the

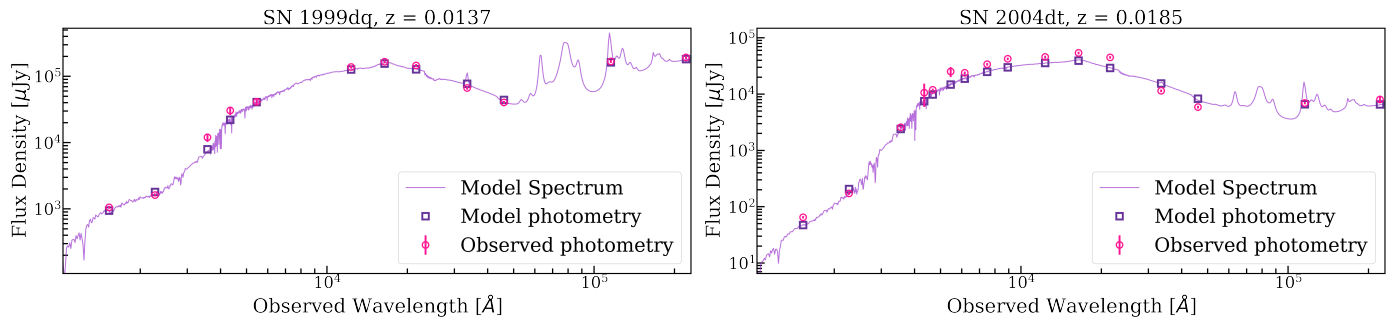


**Fig. 3.** The *Prospector*-produced model spectra (purple lines) and photometry (purple squares) in comparison to the observed photometry (red circles) for two representative SNe Ia in our sample: low velocity SN 1999dq (left) and high velocity SN 2004dt (right). The model SEDs are produced at the median of each hosts’ posterior distributions for their stellar population properties (Table C.1). We showcase these fits to highlight the consistency of the model SED with the observed data, which leads to well-defined posterior distributions for their stellar population properties.

**Table 1.** Stellar Population Properties for SNe Host Samples

Sample	SF	T	Q	$z$	$t_m$ [Gyr]	$\log(M_*/M_\odot)$	SFR [ $M_\odot/\text{yr}$ ]	$\log(\text{sSFR})$ [ $\text{yr}^{-1}$ ]	$\log(Z_*/Z_\odot)$	$A_V$ [mag]
High Velocity	57%	14%	29%	$0.0158^{+0.0094}_{-0.0095}$	$2.95^{+6.88}_{-2.49}$	$10.14^{+0.61}_{-0.5}$	$0.49^{+5.9}_{-0.48}$	$-10.17^{+1.08}_{-2.31}$	$-0.82^{+0.99}_{-0.3}$	$0.55^{+0.9}_{-0.46}$
Low Velocity	70%	5%	25%	$0.0122^{+0.0115}_{-0.0063}$	$1.19^{+4.86}_{-0.75}$	$9.99^{+0.64}_{-0.95}$	$0.37^{+4.31}_{-0.35}$	$-10.09^{+1.21}_{-2.35}$	$-0.83^{+0.8}_{-0.34}$	$0.55^{+1.58}_{-0.47}$
Faint	0%	25%	75%	$0.0041^{+0.0072}_{-0.0014}$	$5.74^{+4.78}_{-4.54}$	$10.1^{+0.65}_{-0.6}$	$0.01^{+0.03}_{-0.01}$	$-12.06^{+1.15}_{-3.26}$	$-0.98^{+1.25}_{-0.19}$	$0.07^{+0.02}_{-0.05}$

**Notes.** The star-forming (SF), transitioning (T), and quiescent (Q) fractions and median and the 16<sup>th</sup>-84<sup>th</sup> percentile region for the redshift and *Prospector*-derived stellar population properties of the hosts of SNe divided into three categories: high velocity, low velocity, and faint SNe.

**Table 2.** Anderson Darling Testing Results

Sample	$z$	$t_m$	$\log(M_*/M_\odot)$	SFR	sSFR	$\log(Z_*/Z_\odot)$	$A_V$	Offset	Na I D
High & Low	0.25	0% (0.22)	0% (> 0.25)	0% (> 0.25)	0% (> 0.25)	0% (> 0.25)	0% (> 0.25)	0.003	27% (0.06)
High & Faint	0.02	0% (> 0.25)	0% (> 0.25)	76% (0.03)	80% (0.1)	0% (> 0.25)	89% (0.01)	0.22	53% (0.003)
Low & Faint	0.05	16% (0.06)	0% (> 0.25)	96% (0.02)	97% (0.04)	0% (> 0.25)	100% (0.0)	> 0.25	13% (0.01)

**Notes.** The results of Anderson Darling testing of the stellar population properties, offsets, and Na I D equivalent widths for pairs of SNe types in this study (high and low velocity SNe, high velocity and faint SNe, and low velocity and faint SNe). We list the percentage of the 5000 tests that reject the null hypothesis ( $P_{AD} < 0.05$ ) for the stellar population properties and Na I D equivalent widths, and within the parentheses we put the  $P_{AD}$  value using distributions constraining the median values for each SN I. We list the  $P_{AD}$  values for the offsets as there are no uncertainties.

host populations of high and low velocity SNe Ia are statistically different, we perform a  $\chi^2$  contingency test using the Python function in the *scipy* package. We assume a null hypothesis that high and low velocity SNe Ia have consistent star forming, transitioning, and quiescent fractions. We determine a  $p$ -value of 0.45, which is much greater than the result needed to reject the null hypothesis ( $< 0.05$ ). We further perform the same tests for both populations in comparison to the full SNe host sample, finding  $p$ -values  $> 0.70$  for both tests. Thus, we determine that the respective star-forming fractions of the high and low velocity SNe Ia hosts are consistent with each other and with the general population.

We further analyze the hosts by comparing their specific star formation rates (sSFRs) versus stellar mass. We compare how these properties populate the star-forming main sequence (SFMS), a well-studied galaxy relation that tracks the SFRs of star-forming galaxies as they gain stellar mass (Whitaker et al. 2014; Speagle et al. 2014; Leja et al. 2022). How transient hosts track the SFMS has important implications for the environmental conditions their progenitor traces (e.g. dependencies on bursts of star formation or the amount of stellar mass). In Figure 4, we plot the sSFRs and stellar masses of the SNe hosts in each of the

three categories, along with the SFMS derived in Leja et al. (2022) for  $z < 0.5$ . This SFMS was derived from a population of galaxies in the COSMOS-2015 and 3D-HST surveys with stellar population modeling fitting from *Prospector*, thus is comparable to our results (Leja et al. 2022). We choose to use the sSFR as opposed to the SFR, as it normalizes the amount of star formation per stellar mass unit, which is useful when comparing galaxies across large stellar mass ranges. We find that both the high and low velocity SNe Ia populate the entire SFMS and are not clustered into any particular combination of sSFR and stellar mass. This, thus, implies that both of their progenitors depend on a wide array of environmental factors, suggesting a breadth of possible host environments and connections recent star formation activity. Interestingly, for both host samples, we do find that at  $\lesssim 10^9 M_\odot$ , all hosts lie above the SFMS. It is not clear whether this is an artifact of the galaxy-targeted nature of the LOSS survey or a real progenitor effect (i.e., high and low velocity SNe Ia progenitors are not as capable of forming in low mass, low sSFR galaxies). While it is a small sample size, our faint SNe sample all fall below the SFMS and reside in higher stellar mass galaxies. If representative of the entire faint SNe sample, this would imply that the faint SNe progenitor is more apparently connected

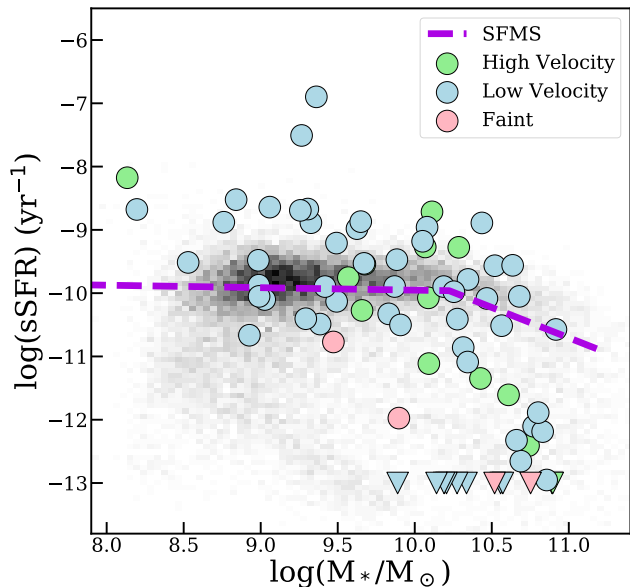


**Fig. 4.** The sSFRs and stellar masses for the hosts of SNe divided into three categories: high velocity (green), low velocity (blue), and faint SNe (pink). Downward arrows represent upper limits. We find that both high and low velocity explosions populate nearly the entire SFMS (purple line; Leja et al. 2022), implying their progenitors have breadth of possible host environments with an array of connections to recent star formation activity. We plot the COSMOS2015 field galaxy population (Laigle et al. 2016) in the background to show the scatter along the SFMS.

to stellar mass rather than star formation (and therefore likely has an older stellar progenitor).

We next compare cumulative distribution functions (CDFs) of SFR between the three categories of SNe and their hosts. We build the CDFs by randomly drawing 5000 values from each host’s *Prospector*-derived posterior distribution for each property. We note that there is no change in the results if we increase beyond 5000 draws. We then build 5000 CDFs for each SN category, as shown in Figure 5. We compare all CDFs through an AD test, with the null hypothesis that the hosts are all derived from the same SFR distribution, and calculate the percentage of tests with a probability  $P_{AD} < 0.05$  and list these values in Table 2. We also list the  $P_{AD}$  determined from distributions built from the median SFR of each SN in Table 2. We choose these comparison methods to encapsulate the uncertainty in the posterior distributions for each SN Ia sub-class. However, we caution that this will not take any uncertainty from the sample sizes of each SN Ia sub-class into account, which may be important in the case of the faint SNe Ia that have a significantly smaller sample size than the other two subclasses. We find that when comparing the SFRs of high and low velocity SNe Ia hosts, 0% of AD tests result in a rejection of the null hypothesis, with the same result being found when comparing sSFRs. We thus infer that if the high and low velocity SNe Ia represent different progenitors, neither progenitor is more dependent on the amount of recent star formation in their environment and thus, the amount of global star formation in a host cannot be used to distinguish these SN populations. Meanwhile, the null hypothesis can be rejected in 76% (80%) and 96% (97%) of

the SFR (sSFR) tests for the faint SNe and high velocity SNe Ia hosts (faint SNe and low velocity SNe Ia hosts). This implies that the faint SNe progenitor is less dependent on recent star formation than either the high or low velocity SNe Ia, if the population studied here is representative of the full faint SNe population. Overall, these results point to the fact that we cannot separate high and low velocity SNe Ia from the amount of global star formation in their hosts, although we note that locally they may indeed trace different star formations.

#### 4.3. Stellar Mass, Age, Metallicity, and Dust

We next compare the main stellar population properties (stellar mass, stellar metallicity, stellar age, total dust) of each SN group’s hosts. We show the  $M_B$  vs. Si 2 velocity relation of the SNe colored by the median stellar mass, stellar population age, stellar metallicity, and dust from the *Prospector* posterior distributions of their hosts in Figure 6. We list the derived median and the 16<sup>th</sup>-84<sup>th</sup> percentile region for each SN category in Table 1. We find that there is very little difference in stellar population property compared to SN type. However, as the faint SNe are almost exclusively in non-star forming hosts, they reside in older galaxies with lower dust and higher stellar mass than the hosts of the other SN types. Furthermore, we see little evidence that the peak *B*-band luminosity and Si 2 velocities are correlated at all with host galaxy stellar population properties.

In Figure 5, we compare the CDFs of each stellar population property for the three SN categories (see Section 2) and compare the distributions through AD tests, results of which are listed in Table 2. We cannot reject the null hypothesis for any of our comparisons in stellar mass and stellar metallicity. This implies that all SNe samples are consistent with having common stellar mass and stellar metallicity distributions. This consistency in the stellar mass distributions between high and low velocity SNe Ia hosts deviates from the conclusion found in Pan (2020), in which all high velocity SNe Ia (defined as having Si II velocities  $> 12,000 \text{ km s}^{-1}$ , at  $z < 0.19$  were found in galaxies with  $> 10^{9.6} M_{\odot}$  and preferentially occurred in more massive galaxies than low velocity SNe Ia. Similar results to Pan (2020) were found in Dettman et al. (2021). In this work, we find one high velocity SN Ia host lower than this stellar mass minimum, at  $\approx 10^{8.1} M_{\odot}$  (the host of SN 2007qe, which was not included in the Pan 2020 sample and had no stellar mass estimate in Dettman et al. 2021), thus this is likely driving the stellar mass distributions to be more similar. We also note that the stellar mass estimates determined in this work are all  $\approx 0.3$  dex smaller than the masses determined in Pan (2020) between the 10 shared hosts, which is a known effect when switching from a Salpeter IMF (used in Pan 2020) to a Chabrier IMF (this work). However, most importantly, the difference will only affect individual stellar mass measurements and not how the distributions of stellar masses compare. Thus, the similarity of the stellar mass distributions between high and low velocity SNe Ia found in this work is real, and not simply caused by a different stellar population modeling technique or SED fitting tool. Interestingly, the Pan (2020) and Dettman et al. (2021) studies are both based on larger SNe host samples, from e.g., the Foundation Supernova Survey (Foley et al. 2018) and the PTF survey, which should better target SNe

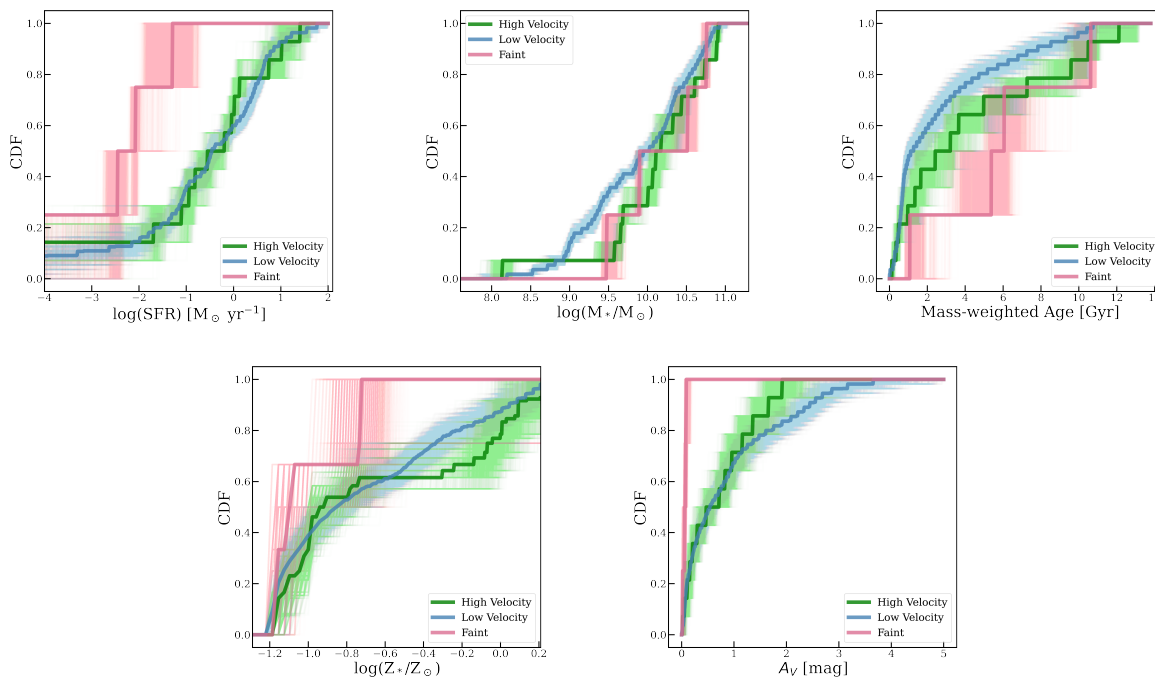


**Fig. 5.** From left to right, top to bottom: The cumulative distribution (CDF) and 5000 realizations on the CDF for the SFRs, stellar mass ( $\log(M/M_\odot)$ ), mass-weighted age, stellar metallicity ( $\log(Z_*/Z_\odot)$ ), and total  $A_V$  of high velocity (green), low velocity (blue), and faint SNe (pink) hosts. The darker colors represent the median CDF. We find that there is very little difference in stellar population properties between the high and low velocity SNe Ia hosts, suggesting that global host properties alone cannot be used to separate these SN classes or distinguish different progenitor types.

in lower mass galaxies than the LOSS survey used in this work (Pan et al. 2015; Graur et al. 2017). Thus, this current discrepancy highlights the need for further, uniform host studies with larger SN samples to more robustly determine whether high velocity SNe Ia do occur significantly in lower mass galaxies. At this time, our results may simply show that high velocity SNe Ia can occur in a more diverse array of environments than previously known.

For mass-weighted age, we can reject 0% of tests between high and low velocity SNe Ia hosts and 16% of tests between low velocity and faint SNe hosts. The null hypothesis cannot be rejected in any of the trials between high velocity and faint SNe hosts. Furthermore, we find that 0% of tests can be rejected between  $A_V$  distributions between the high and low velocity SNe Ia hosts. However, as the faint SNe hosts tend to have very little dust, we find that 89% of AD tests can be rejected between faint SNe and high velocity SNe Ia host  $A_V$  distributions, and 100% of tests can be rejected between faint SNe and low velocity SNe Ia host  $A_V$  distributions. We do note, once again, that the faint SNe sample size is small, thus these conclusions are only substantiated if they are representative of their entire population.

Overall, we find very little evidence for significant stellar population property difference between high and low velocity SNe Ia populations, suggesting the global environment alone cannot distinguish the two SNe and that their progenitors’ environments have similar stellar population properties. Furthermore, this suggests that the differences in SN properties of either group cannot be explained by differences in their global host environments. We find more substantial evidence that the environments of faint SNe are quite different, however note that the population of faint

SNe we have explored in this paper is quite small thus might not be fully representative of the host properties of all faint SNe.

## 5. Evidence for Difference in Local Environments

As discussed in the previous section, we find little evidence that the global environmental properties of possible high and low velocity SNe are different. In this section, we discuss if their progenitors are tracing different local environments through analyzing their observed physical offset distributions and Na I D equivalent widths.

### 5.1. Offsets

The offsets of transients from the center of their host galaxies has been used to probe local environments, migrations from progenitor birthplaces, and other key factors that help distinguish transient types and progenitors (e.g. Kasliwal et al. 2012; Blanchard et al. 2016; Fong et al. 2022). Thus, we determine if the SNe Ia sub-classes studied here have distinct offset distributions. We obtain angular separations of our SNe sample to the center of their hosts and the 2MASS K-band “total” radii of the host galaxies, which is available for 69 out of the 74 host studied in this work (13/14 high velocity SNe Ia and 52/56 of the low velocity SNe Ia hosts) from NED. The 2MASS K-band “total” radius is defined as the isophotal radius (the semi-major axis at 20 mag/arcsec<sup>2</sup> isophote at Ks) added to the integration of the surface brightness profile that extends from the isophotal aperture out to  $\sim 4$  disk scale lengths. This radius is typically 10-20% larger than the isophotal radius (Skrutskie et al. 2006). We determine host-normalized off-

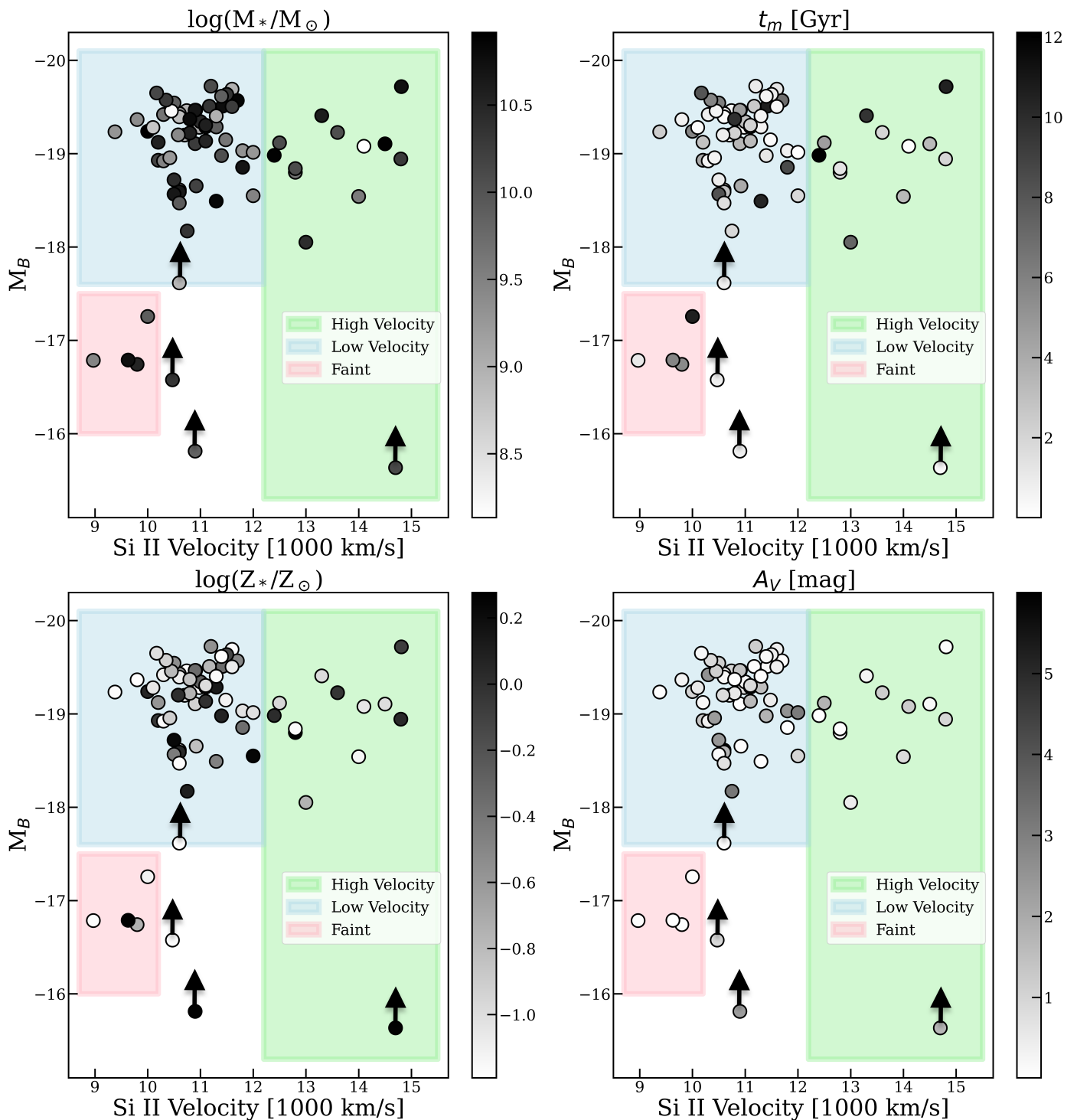


**Fig. 6.** The same plot as in Figure 1, with SNe colored by their hosts’ amount of stellar mass ( $\log(M/M_{\odot})$ , top left), mass-weighted age ( $t_m$ , top right), stellar metallicity ( $\log(Z_*/Z_{\odot})$ , bottom left), and total  $A_V$  (bottom right). We find that there appears very little correlation between host stellar population property and SN property.

sets, or the relative location of the SN within its host, by dividing the angular separation of each SNe to their hosts’ centers by the host galaxies’ size. We find a median and the 16<sup>th</sup>-84<sup>th</sup> percentile region for host-normalized offsets to be  $0.19^{+0.99}_{-0.08} r/r_e$  for high velocity SNe Ia hosts,  $0.53^{+0.61}_{-0.29} r/r_e$  for low velocity SNe Ia hosts, and  $0.4^{+0.1}_{-0.11} r/r_e$  for faint SNe, and we show the respective CDFs in Figure 7. When conducting an AD test between pairs of the three SNe off-

set distributions, we find that we cannot reject the null hypothesis for any pair ( $P_{AD} \geq 0.20$ ) except the high and low velocity SNe Ia ( $P_{AD} = 0.003$ ), as high velocity SNe Ia are more concentrated towards the center of their hosts than low velocity SNe Ia. These results are in agreement with those in Wang et al. (2013) (52% of our SNe sample overlaps with this sample), which studied the relative locations of high and low velocity SNe Ia within their hosts, finding high velocity SNe Ia occur at lower radial distances. Future



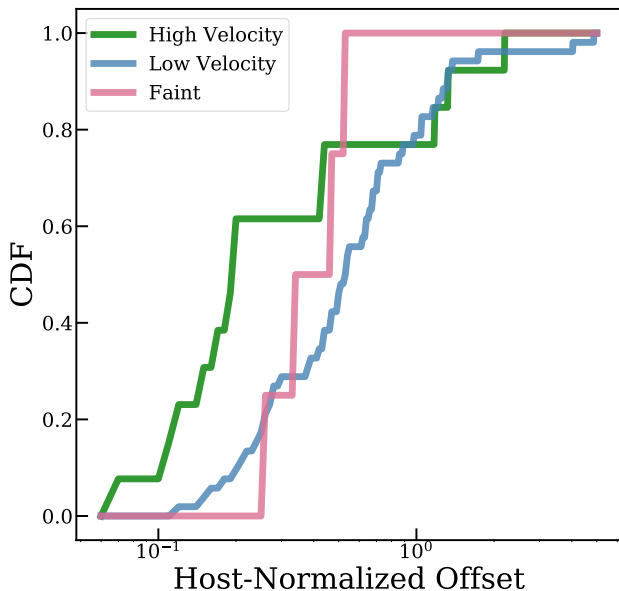


**Fig. 7.** CDFs of the host-normalized offsets (physical offset of SNe from the center of the host normalized by the  $K$ -band total radius) for the high velocity (green), low velocity (blue), and faint SNe (pink) classifications. High velocity SNe Ia have smaller host-normalized offsets than either low velocity or faint SNe, implying they lie more towards the center of their hosts than the other SN sub-classes. This may be indicative of a distinct local environment.

studies focused on spectral emission at these locations (such as star formation tracers like  $H\alpha$ ) may reveal if these offsets are indicative of a local stellar population property difference. Furthermore, the difference in offset distributions could indicate that high velocity SNe Ia appear redder from extinction in their local environments, as more gas and dust lies towards the center of the galaxies. Overall, these results highlight that while global properties of high and low velocity SNe Ia may not be distinguished, the local environments may play a larger role in separating these sub-classes.

## 5.2. Na I D Equivalent Widths

Finally, we analyze the equivalent widths of the Na I D lines in each SN spectrum to infer if high and low velocity SNe Ia probe different circumstellar or interstellar environments. The Na I D line strength probes the host dust and circumstellar gas, dust, and metals (Blondin et al. 2009; Folatelli et al. 2010; Poznanski et al. 2012; Phillips et al. 2013), thus is a good indicator of the local environment surrounding the SN (Sternberg et al. 2011a, 2014). We collect published Na I D equivalent widths for 61 SNe in Wang et al. (2019) and references therein. For the 13 remaining SNe: 1990N (Jeffery et al. 1992; Gómez & López 1998), 1991bg (Filippenko et al. 1992), 2005hk (Phillips et al. 2007), 2000E, 2006ax, 2006lf, 2008Q (Blondin et al. 2012), 2000dr, 2002cs, 2003Y, 2003gn, 2003gt, 2007on (Silverman et al. 2012), we collect spectra from WISeREP (Yaron & Gal-Yam 2012). To determine the Na I D equivalent widths for these SNe Ia, we performed a standard equivalent width measurement on these mostly lower resolution spectra as seen in Figure 8. In the case where a SN has multiple high signal-to-noise spectra, we measured the equivalent width on each spectrum and combined the individual equivalent

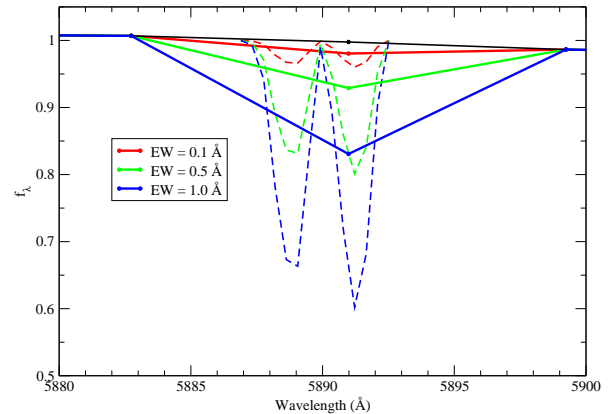


**Fig. 8.** An example measurement of the equivalent width on the day +4 spectrum of SN 1990N (one of the lowest resolution spectra in our sample; Leibundgut et al. 1991) seen in black. An upper limit of 0.1 Å can be placed on this individual spectrum. We present example strengths of the lines at 0.1, 0.5 and 1.0 Å in both high-resolution (dashed) and at the resolution these Na I D lines would have in the lower resolution of the observed spectrum of SN 1990N (in solid red, green, and blue respectively). The noise for each measurement is taken directly from that reported by the observer or estimated from the signal-to-noise of the continuum around this feature. In the above case, the error bars are equal to the line width,  $S/N \sim 100$  per resolution element, which is the typical for many of these nearby SNe Ia. All measurements include the uncertainty in the continuum which is very small given the short wavelength range covered by these features.

measurements, weighted by their uncertainties, to provide a single equivalent width and uncertainty for each SN. We note that in all but two cases (SNe 2006lf and 2007on), they are upper limits. We determine median and the 16<sup>th</sup>-84<sup>th</sup> percentile regions of the Na I D equivalent widths for each SN Ia sub-class. We find that high velocity SNe Ia have Na I D equivalent widths  $0.62^{+0.95}_{-0.55}$  Å, low velocity SNe Ia have equivalent widths  $0.22^{+0.61}_{-0.19}$  Å, and faint SNe have equivalent widths  $0.07^{+0.09}_{-0.05}$  Å.

To make CDFs of the Na I D equivalent widths, we build Gaussian distributions using their median and  $1\sigma$  uncertainties, with a minimum possible value of 0 Å, and sample from this distribution 5000 times. We show the median and the 16<sup>th</sup>-84<sup>th</sup> percentile region for these CDFs in Figure 9. We compare pairs of the 5000 CDFs and list the percentage of tests that reject the null hypothesis in Table 2. We find that we can reject the null hypothesis in 27% of the tests between high and low velocity SNe Ia, 53% of tests between high velocity and faint SNe, and 13% of tests between low velocity and faint SNe. Thus, there is little statistical evidence that high and low velocity SNe Ia have different Na I D equivalent widths.

## 6. Discussion

In this work, we have focused on the global host galaxy and local environmental properties of high and low velocity SNe Ia to see if we can find evidence for an environmental condition that could explain why high velocity SNe Ia appear redder. While we find no evidence that the global host

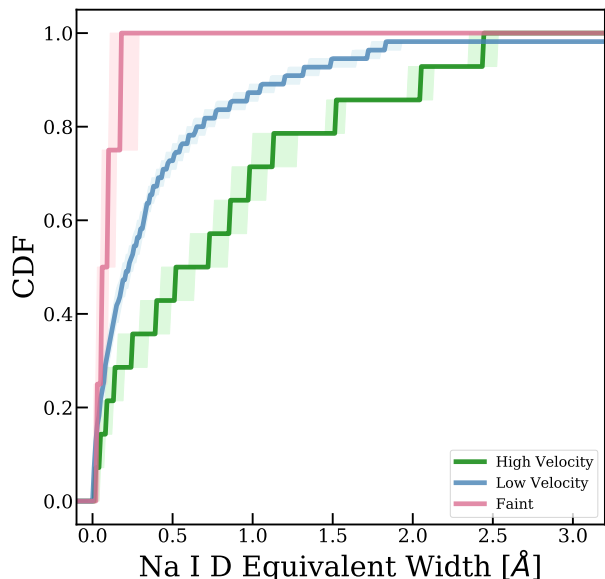


**Fig. 9.** CDFs on the Na I D line equivalent widths for high velocity (green), low velocity (blue), and faint (pink) SNe. Darker lines represent the median of the distribution and lighter lines represent uncertainty on the CDF. We cannot reject the null hypothesis that high and low velocity SNe Ia have similar Na I D equivalent width distributions with AD statistical tests.

properties can account for these differences in SN observables, we have shown that more locally, using the host normalized offsets, high and low velocity SNe Ia environments may indeed differ. We also note that while we did not find statistical support for different Na I D equivalent width distributions between high and low velocity SNe Ia, with even a minimally larger high velocity SN sample, these distributions may indeed become distinct. For example, if there were only 1-2 more high velocity SNe Ia that showed Na I D equivalent width strengths at the median of the population studied here,  $> 50\%$  of Anderson Darling tests would be rejected between high and low velocity SNe Ia. At the minimum, this signifies a need for larger samples of these SNe Ia sub-classes from volume-limited surveys that are not biased against finding more extinct, centrally located SNe Ia, for more robust statistical tests. At most, the potential difference in both host-normalized offsets and Na I D equivalents could have major implications for whether the environment or the progenitor causes high velocity SNe Ia to have redder colors, which we briefly discuss below.

Understanding the contribution of the local environmental properties versus the progenitor properties to the redness of high velocity SNe Ia requires discerning whether the excess Na I D gas possibly observed in high velocity SNe comes from the circumstellar or interstellar medium. Indeed, Phillips et al. (2013), which explored the properties of SNe Ia as a function of both the diffuse interstellar bands (DIBs) and Na I D lines through high-resolution spectroscopy, found that (i) the low  $R_V$  values derived for very reddened SNe Ia are likely caused by dust in the interstellar medium, and not the circumstellar medium, and (ii) that nearly a quarter of SNe Ia have large host Na I column densities in comparison with the amount of dust observed to redden their spectra. Phillips et al. (2013) fur-

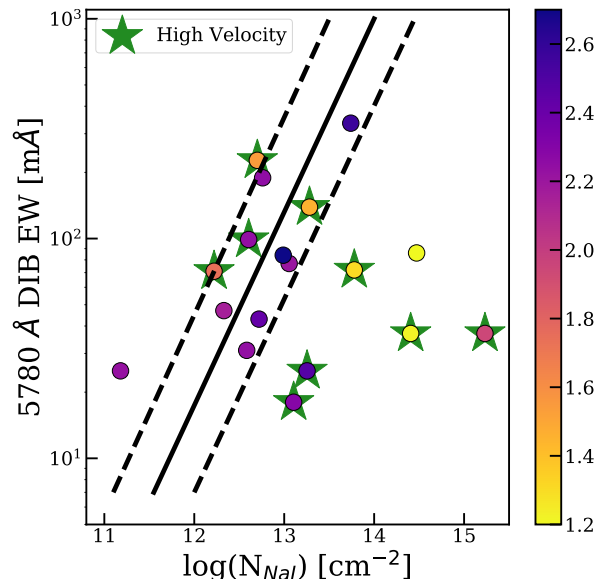


**Fig. 10.** The equivalent width of the 5780 Å DIB vs. column depth of Na I for those SNe Ia from Phillips et al. (2013) that we can separate between low and high velocity. We have color coded the data points by their assumed  $R_V$ . We note that uncertainties are smaller than symbols. The black line represents the correlation found in the Milky Way galaxy and the dashed black represent the  $1\sigma$  uncertainty on the relation. While all but two of the low velocity SNe Ia fall within the  $1\sigma$  region of the Milky Way relation, over half the high velocity SNe Ia fall outside this correlation.

ther noted that all of the SNe Ia with unusually strong Na I D lines have “blueshifted” profiles in the classification scheme following (Sternberg et al. 2011b) and that the majority of the high velocity SNe Ia (seven out of ten) have this “blueshifted” feature. This paper, however, relies on one major assumption: that the intrinsic colors of both the high and low velocity SNe Ia are similar as defined by the SNooPy algorithm (Burns et al. 2011). Here, we revisit these conclusions given more recent work on the potential origins of these two sub-groups of SNe Ia.

Indeed, there already exists theoretical evidence that high and low velocity SNe Ia may have different intrinsic colors caused by separate progenitors. For example, Polin et al. (2019) suggests that the redder colors of high velocity SNe Ia are a natural consequence of a sub- $M_{\text{ch}}$  mass explosion, while the bluer colors of low velocity SNe Ia are due to classical  $M_{\text{ch}}$  explosions. We note that while others claim that the bulk of the low velocity SNe Ia can also derive from sub- $M_{\text{ch}}$  explosions (Shen et al. 2021), we use the Polin et al. (2019) model to guide our discussion and simply note that this relationship implies that we are seeing at least two separate progenitor systems and/or explosion mechanisms with *intrinsically* different colors. Nonetheless, this only strengthens the findings in Phillips et al. (2013) as the anomalously low values of  $R_V$  they found for reddened SNe Ia would become even lower and the lack of correlation between the strength of the Na I D lines and the DIBs, or assumed dust from the underlying colors, would become even smaller. An example of this can be seen in Figure 10.

Here, we plot the equivalent width of the 5780 Å DIB versus column depth of Na I for those SNe Ia from Phillips et al. (2013) that we can separate between low and high velocity. While all but one of the low velocity SNe Ia tightly follow the correlation found in the Milky Way galaxy, nearly half the high velocity SNe Ia lie outside this correlation. Such a result strongly implies that the dust is a property of the ISM and furthermore that the CSM of these events is almost certainly contributing a clear excess to the Na I D profiles (Maguire et al. 2013; Phillips et al. 2013). Maguire et al. (2013) further found that SNe Ia with blueshifted Na I D profiles had both an excess absorption compared to those with non-blueshifted profiles and redder  $B - V$  colors at peak brightness.

While we have only considered three sub-groups of SNe Ia with simple velocity and peak brightness cuts, we note that the sub- $M_{\text{ch}}$  models of Polin et al. (2019) extend down to more normal velocities ( $v \sim 10,750$  km/s) and slightly fainter peak absolute magnitudes ( $B \sim -18.5$ ). It would be interesting to see in a future, larger, volume limited, sample if the blueshifted SNe Ia noted by Maguire et al. (2013) and Phillips et al. (2013) shared the characteristics of this sub-population of SNe Ia. Additional future work is also needed to understand how the more local environments of these sub- $M_{\text{Ch}}$  explosion candidates may further affect their colors and SN observables, as we have noted how high velocity SNe Ia trend towards smaller offsets from their hosts' centers and are thus likely more observationally affected by extinction due to their more central locations.

## 7. Conclusions

In this study, we have determined the host galaxy stellar population properties for 74 SNe Ia at  $z < 0.04$ , divided into the sub-categories of high velocity, low velocity, and faint SNe Ia based on their peak  $B$ -band luminosities and Si 2 velocities. All SNe Ia have good photometric coverage for determination of their properties and their host galaxies have at least three bands of archival photometry, the minimum requirement for a stellar population fit. We summarize our main conclusions below:

- We find that there is no statistical evidence for differences between the high velocity (Si 2 velocities  $\gtrsim 12,200$  km s $^{-1}$ ) and low velocity SNe Ia host galaxy populations in SFR, sSFR, stellar mass, stellar population age, dust attenuation, and stellar metallicity. Within the small sample used in this paper, the fainter ( $M_B > -17.5$  mag) SNe occur in older, more massive, and more quiescent galaxies than the rest SNe population.
- In our comparison between the host-normalized offsets for the SNe (from SN position to center of the host), we find high velocity SNe Ia are more concentrated towards the center of their hosts than low velocity SNe Ia. This suggests that there may be local environmental differences between these populations that are not distinct in their global properties.
- Finally, we find that high velocity and low velocity SNe Ia do not have statistically different Na I D EW distributions, implying there is little evidence that surrounding Na gas is affecting the observable differences of these populations.

Our results on the stellar population properties of SNe Ia hosts strongly suggest that the global environments of high and low velocity SNe Ia are not intrinsically different. While this might be a cause of the galaxy-targeted nature of the SNe Ia survey we used, which generally has more limitations in the host types (e.g. more massive galaxies; Pan et al. 2015), we have also shown that high velocity SNe Ia are capable of occurring in more diverse and less massive hosts than studies focused on SNe Ia samples without this survey bias (Pan 2020; Dettman et al. 2021). We do, however, find that the smaller host-normalized offsets of high velocity SNe Ia may show that the local environments between these populations are different. Future work necessitates the use of high-resolution photometry and/or Integral Field Unit (IFU) spectroscopy to resolve the local environments of nearby high velocity SNe Ia to more conclusively determine if these offsets are indicative of separate environmental properties than more normal velocity SNe Ia and more conclusively inform if the Na I D gas in high velocity SNe Ia is interstellar or circumstellar. Indeed, Rigault et al. (2020) has already shown that the local star formation activity surrounding SNe Ia does affect the corrections to their peak magnitudes used in the standardization process for cosmology. Furthermore, it has been proposed that sub- $M_{\text{ch}}$  progenitors are likely more connected to star formation and occur in younger stellar population than classical SNe Ia (de los Reyes et al. 2020). Thus, if high velocity SNe Ia do trace younger and more star-forming regions within their hosts, it may be indicative of their possible sub- $M_{\text{ch}}$  progenitor, as proposed by Polin et al. (2019).

Our conclusions notably highlight that the global stellar population properties cannot be used to separate classes of SNe Ia for future cosmology measurements. This is especially problematic for the upcoming era of the Vera Rubin Observatory (VRO), in which hundreds of thousands of SNe Ia will be discovered, the majority of which will not be followed up with spectroscopy of the supernova to determine their Si 2 velocities. Furthermore, if the local environments of high velocity SNe are indeed different then these environmental differences may only be probed for more local universe events where resolving stellar populations within a galaxy is possible. At higher redshifts, where the majority of SNe will be discovered, such observations are not feasible. This, in effect, would lead to more contamination from these events in the population used for cosmology.

As separating SNe Ia by their global and/or local stellar population properties is extremely difficult, if not impossible, and obtaining a spectrum for the majority of SNe discovered by the VRO is too ambitious, a more concerted effort needs to be placed on distinguishing SNe Ia based on their photometric properties. Indeed, most current methods using SNe Ia as probes for cosmology impose a color cut using SALT2 of  $|c| \lesssim 0.3$  (similar to a cut in  $B - V$ ; Smith et al. 2020; Popovic et al. 2021). As strong Na I D lines imply redder SN, either due to actual extinction or association with the intrinsically redder sub-group of high velocity SNe Ia, we can use this knowledge to make more informed color cuts such that high velocity SNe Ia are not included in the cosmology sample. Furthermore, if future analyses find that the "blueshifted" Na I D subset of SNe Ia include both the high and lower velocity SNe Ia that follow the Polin et al. (2019) Si II velocity versus peak brightness

relationship, then slightly more complicated cuts will be required. The upcoming release of the ZTF DR2 SNe Ia sample, comprised of over 3000 SNe, will greatly improve our understanding of these relationships (Rigault et al. 2024).

## Acknowledgements

We thank Adam Miller and Wen-fai Fong for valuable comments and suggestions. A.E.N. acknowledges support from the Henry Luce Foundation through a Graduate Fellowship in Physics and Astronomy. The Fong Group at Northwestern acknowledges support by the National Science Foundation under grant Nos. AST-1814782, AST-1909358 and CAREER grant No. AST-2047919. Funding for this research came from the Director, Office of Science, Office of High Energy Physics of the U.S. Department of Energy under Contract no. DE-AC02-05CH1123. The National Energy Research Scientific Computing Center, a DOE Advanced Scientific Computing User Facility under the same contract, provided staff, computational resources, and data storage for this project.

This research has made use of the NASA/IPAC Extragalactic Database, which is funded by the National Aeronautics and Space Administration and operated by the California Institute of Technology.

This research was supported in part through the computational resources and staff contributions provided for the Quest high performance computing facility at Northwestern University, which is jointly supported by the Office of the Provost, the Office for Research, and Northwestern University Information Technology.

## References

- Ahumada, R., Prieto, C. A., Almeida, A., et al. 2020, *ApJS*, 249, 3
- Benetti, S., Cappellaro, E., Mazzali, P. A., et al. 2005, *ApJ*, 623, 1011
- Bennett, C. L., Larson, D., Weiland, J. L., & Hinshaw, G. 2014, *ApJ*, 794, 135
- Blakeslee, J. P., Cantiello, M., Mei, S., et al. 2010, *ApJ*, 724, 657
- Blanchard, P. K., Berger, E., & Fong, W.-f. 2016, *ApJ*, 817, 144
- Blondin, S., Matheson, T., Kirshner, R. P., et al. 2012, *AJ*, 143, 126
- Blondin, S., Prieto, J. L., Patat, F., et al. 2009, *ApJ*, 693, 207
- Bouquin, A. Y. K., Gil de Paz, A., Muñoz-Mateos, J. C., et al. 2018, *ApJS*, 234, 18
- Brout, D. & Scolnic, D. 2021, *ApJ*, 909, 26
- Bulla, M., Miller, A. A., Yao, Y., et al. 2020, *ApJ*, 902, 48
- Burns, C. R., Stritzinger, M., Phillips, M. M., et al. 2011, *AJ*, 141, 19
- Burrow, A., Baron, E., Ashall, C., et al. 2020, *ApJ*, 901, 154
- Byler, N., Dalcanton, J. J., Conroy, C., & Johnson, B. D. 2017, *ApJ*, 840, 44
- Calzetti, D., Armus, L., Bohlin, R. C., et al. 2000, *ApJ*, 533, 682
- Cardelli, J. A., Clayton, G. C., & Mathis, J. S. 1989, *ApJ*, 345, 245
- Chabrier, G. 2003, *PASP*, 115, 763
- Childress, M., Aldering, G., Antilogus, P., et al. 2013, *ApJ*, 770, 108
- Conroy, C. & Gunn, J. E. 2010, *ApJ*, 712, 833
- Conroy, C., Gunn, J. E., & White, M. 2009, *ApJ*, 699, 486
- Contreras, C., Hamuy, M., Phillips, M. M., et al. 2010, *AJ*, 139, 519
- D’Andrea, C. B., Gupta, R. R., Sako, M., et al. 2011, *ApJ*, 743, 172
- de los Reyes, M. A. C., Kirby, E. N., Seitzzahl, I. R., & Shen, K. J. 2020, *ApJ*, 891, 85
- Dettman, K. G., Jha, S. W., Dai, M., et al. 2021, *ApJ*, 923, 267
- Dilday, B., Howell, D. A., Cenko, S. B., et al. 2012, *Science*, 337, 942
- Draine, B. T. & Li, A. 2007, *ApJ*, 657, 810
- Falcón-Barroso, J., Sánchez-Blázquez, P., Vazdekis, A., et al. 2011, *A&A*, 532, A95
- Filippenko, A. V., Li, W. D., Treffers, R. R., & Modjaz, M. 2001, in *Astronomical Society of the Pacific Conference Series*, Vol. 246, IAU Colloq. 183: Small Telescope Astronomy on Global Scales, ed. B. Paczynski, W.-P. Chen, & C. Lemme, 121
- Filippenko, A. V., Richmond, M. W., Branch, D., et al. 1992, *AJ*, 104, 1543
- Folatelli, G., Phillips, M. M., Burns, C. R., et al. 2010, *AJ*, 139, 120
- Foley, R. J. & Kasen, D. 2011, *ApJ*, 729, 55
- Foley, R. J., Scolnic, D., Rest, A., et al. 2018, *MNRAS*, 475, 193
- Fong, W.-f., Nugent, A. E., Dong, Y., et al. 2022, *ApJ*, 940, 56
- Frohmaier, C., Sullivan, M., Nugent, P. E., Goldstein, D. A., & DeRose, J. 2017, *ApJS*, 230, 4
- Gallazzi, A., Charlot, S., Brinchmann, J., White, S. D. M., & Tremonti, C. A. 2005, *MNRAS*, 362, 41
- Goldstein, D. A. & Kasen, D. 2018, *ApJ*, 852, L33
- Gómez, G. & López, R. 1998, *AJ*, 115, 1096
- Graur, O., Bianco, F. B., Huang, S., et al. 2017, *ApJ*, 837, 120
- Guillochon, J., Parrent, J., Kelley, L. Z., & Margutti, R. 2017, *ApJ*, 835, 64
- Gupta, R. R., D’Andrea, C. B., Sako, M., et al. 2011, *ApJ*, 740, 92
- Harris, C. E., Nugent, P. E., Horesh, A., et al. 2018, *ApJ*, 868, 21
- Hicken, M., Challis, P., Jha, S., et al. 2009, *ApJ*, 700, 331
- Hinshaw, G., Larson, D., Komatsu, E., et al. 2013, *ApJS*, 208, 19
- Howell, D. A., Sullivan, M., Nugent, P. E., et al. 2006, *Nature*, 443, 308
- Hsiao, E. Y., Hoeflich, P., Ashall, C., et al. 2020, *ApJ*, 900, 140
- Jeffery, D. J., Leibundgut, B., Kirshner, R. P., et al. 1992, *ApJ*, 397, 304
- Johnson, B. D., Leja, J., Conroy, C., & Speagle, J. S. 2021, *ApJS*, 254, 22
- Kasliwal, M. M., Kulkarni, S. R., Gal-Yam, A., et al. 2012, *ApJ*, 755, 161
- Kelly, P. L., Hicken, M., Burke, D. L., Mandel, K. S., & Kirshner, R. P. 2010, *ApJ*, 715, 743
- Kriek, M. & Conroy, C. 2013, *ApJ*, 775, L16
- Laigle, C., McCracken, H. J., Ilbert, O., et al. 2016, *ApJS*, 224, 24
- Lampeitl, H., Smith, M., Nichol, R. C., et al. 2010, *ApJ*, 722, 566
- Leaman, J., Li, W., Chornock, R., & Filippenko, A. V. 2011, *MNRAS*, 412, 1419
- Leibundgut, B., Kirshner, R. P., Filippenko, A. V., et al. 1991, *ApJ*, 371, L23
- Leja, J., Johnson, B. D., Conroy, C., Dokkum, P. G. v., & Byler, N. 2017, *The Astrophysical Journal*, 837, 170
- Leja, J., Speagle, J. S., Ting, Y.-S., et al. 2022, *ApJ*, 936, 165
- Liu, C., Miller, A. A., Polin, A., et al. 2023, *ApJ*, 946, 83
- Macri, L. M., Stetson, P. B., Bothun, G. D., et al. 2001, *ApJ*, 559, 243
- Maguire, K., Sullivan, M., Patat, F., et al. 2013, *MNRAS*, 436, 222
- Mannucci, F., Maoz, D., Sharon, K., et al. 2008, *MNRAS*, 383, 1121
- Maoz, D., Mannucci, F., & Nelemans, G. 2014, *ARA&A*, 52, 107
- Meldorf, C., Palmese, A., Brout, D., et al. 2023, *MNRAS*, 518, 1985
- Mould, J. R., Huchra, J. P., Freedman, W. L., et al. 2000, *ApJ*, 529, 786
- Neill, J. D., Sullivan, M., Howell, D. A., et al. 2009, *ApJ*, 707, 1449
- Ni, Y. Q., Moon, D.-S., Drout, M. R., et al. 2023, *ApJ*, 946, 7
- Nugent, A. E., Fong, W., Dong, Y., et al. 2020, *ApJ*, 904, 52
- Pan, Y.-C. 2020, *ApJ*, 895, L5
- Pan, Y. C., Jheng, Y. S., Jones, D. O., et al. 2022, *arXiv e-prints*, [arXiv:2211.06895](https://arxiv.org/abs/2211.06895)
- Pan, Y. C., Sullivan, M., Maguire, K., et al. 2015, *MNRAS*, 446, 354
- Pan, Y. C., Sullivan, M., Maguire, K., et al. 2014, *MNRAS*, 438, 1391
- Paxton, B., Schwab, J., Bauer, E. B., et al. 2018, *ApJS*, 234, 34
- Perlmutter, S., Aldering, G., Goldhaber, G., et al. 1999, *ApJ*, 517, 565
- Phillips, M. M., Li, W., Frieman, J. A., et al. 2007, *PASP*, 119, 360
- Phillips, M. M., Simon, J. D., Morrell, N., et al. 2013, *ApJ*, 779, 38
- Polin, A., Nugent, P., & Kasen, D. 2019, *ApJ*, 873, 84
- Polin, A., Nugent, P., & Kasen, D. 2021, *ApJ*, 906, 65
- Popovic, B., Brout, D., Kessler, R., Scolnic, D., & Lu, L. 2021, *ApJ*, 913, 49
- Poznanski, D., Prochaska, J. X., & Bloom, J. S. 2012, *MNRAS*, 426, 1465
- Riess, A. G., Filippenko, A. V., Challis, P., et al. 1998, *AJ*, 116, 1009
- Riess, A. G., Yuan, W., Macri, L. M., et al. 2022, *ApJ*, 934, L7
- Rigault, M., Brinnel, V., Aldering, G., et al. 2020, *A&A*, 644, A176
- Rigault, M., Smith, M., Goobar, A., et al. 2024, *A&A*(Submitted)
- Saha, A., Sandage, A., Thim, F., et al. 2001, *ApJ*, 551, 973
- Salim, S., Boquien, M., & Lee, J. C. 2018, *ApJ*, 859, 11
- Scalzo, R. A., Ruiter, A. J., & Sim, S. A. 2014, *MNRAS*, 445, 2535
- Schlafly, E. F. & Finkbeiner, D. P. 2011, *ApJ*, 737, 103
- Shen, K. J., Boos, S. J., Townsley, D. M., & Kasen, D. 2021, *ApJ*, 922, 68
- Shen, K. J., Kasen, D., Miles, B. J., & Townsley, D. M. 2018, *ApJ*, 854, 52
- Silverman, J. M., Foley, R. J., Filippenko, A. V., et al. 2012, *MNRAS*, 425, 1789
- Skrutskie, M. F., Cutri, R. M., Stiening, R., et al. 2006, *AJ*, 131, 1163
- Smith, M., D’Andrea, C. B., Sullivan, M., et al. 2020, *AJ*, 160, 267

- Speagle, J. S. 2020, MNRAS[arXiv:1904.02180]  
Speagle, J. S., Steinhardt, C. L., Capak, P. L., & Silverman, J. D. 2014, ApJS, 214, 15  
Sternberg, A., Gal-Yam, A., Simon, J. D., et al. 2011a, Science, 333, 856  
Sternberg, A., Gal-Yam, A., Simon, J. D., et al. 2011b, Science, 333, 856  
Sternberg, A., Gal-Yam, A., Simon, J. D., et al. 2014, MNRAS, 443, 1849  
Sullivan, M., Conley, A., Howell, D. A., et al. 2010, MNRAS, 406, 782  
Sullivan, M., Le Borgne, D., Pritchett, C. J., et al. 2006, ApJ, 648, 868  
Tacchella, S., Conroy, C., Faber, S. M., et al. 2022, ApJ, 926, 134  
Vincenzi, M., Sullivan, M., Möller, A., et al. 2023, MNRAS, 518, 1106  
Wang, X., Chen, J., Wang, L., et al. 2019, ApJ, 882, 120  
Wang, X., Filippenko, A. V., Ganeshalingam, M., et al. 2009, ApJ, 699, L139  
Wang, X., Wang, L., Filippenko, A. V., Zhang, T., & Zhao, X. 2013, Science, 340, 170  
Whitaker, K. E., Franx, M., Leja, J., et al. 2014, ApJ, 795, 104  
Wright, E. L., Eisenhardt, P. R. M., Mainzer, A. K., et al. 2010, AJ, 140, 1868  
Yaron, O. & Gal-Yam, A. 2012, PASP, 124, 668  
Zheng, W., Kelly, P. L., & Filippenko, A. V. 2017, ApJ, 848, 66  
Zheng, W., Kelly, P. L., & Filippenko, A. V. 2018, ApJ, 858, 104

## Appendix A: Supernova Properties

Here, we record all properties of the SNe Ia studied in this work.

**Table A.1.** Supernova Data

SN Name	Type	$z$	$\mu$	$M_B$	$M_{\sigma,B}$	$B - V$	$v_{SiII}$	$\sigma_{v_{SiII}}$	Offset [kpc]	EW Na I D [Å]	$\sigma_{NaID}$ [Å]	Ref.
1998dh	low	0.009	33.03	-19.14	0.22	0.08	11.1	0.5	10.16	0.36	0.12	1
1998dm	low	0.007	32.25	-17.61	0.28	0.26	10.6	0.3	4.86	0.62	0.13	1
1999cp	low	0.009	33.38	-19.43	0.28	-0.001	10.6	0.3	12.37	0.0	0.08	1
1999dq	low	0.014	33.94	-19.47	0.15	0.11	10.9	0.1	2.17	1.0	0.07	1
1999gp	low	0.027	35.32	-19.34	0.09	-0.01	11.0	0.2	7.77	0.27	0.2	1
2000cx	low	0.008	32.69	-19.57	0.24	0.12	11.7	0.2	16.21	0.0	0.2	1
2000dn	low	0.032	35.74	-19.12	0.07	-0.01	10.2	0.2	18.52	0.0	0.2	1
2000dr	low	0.019	34.55	-18.57	0.11	0.12	10.5	0.3	7.93	0.0 <sup>†</sup>	0.02	1
2000fa	low	0.021	34.9	-19.01	0.10	0.06	12.0	0.2	4.01	0.97	0.19	1
2001en	high	0.016	34.19	-19.12	0.15	0.01	12.5	0.4	8.48	0.98	0.14	1
2001ep	low	0.013	33.79	-18.92	0.15	0.02	10.3	0.3	4.83	0.73	0.2	1
2002bo	high	0.004	31.99	-18.05	0.29	0.39	13.0	0.3	2.1	2.44	0.09	1
2002cr	low	0.009	33.38	-19.20	0.18	-0.03	10.7	0.3	13.58	0.51	0.12	1
2002dj	high	0.009	33.08	-19.11	0.21	0.12	14.5	0.3	2.22	0.8	0.13	1
2002dl	low	0.016	34.32	-18.47	0.12	0.14	10.6	0.4	4.43	0.54	0.17	1
2002eb	low	0.027	35.43	-19.42	0.08	-0.07	10.3	0.4	10.72	0.0	0.2	1
2002er	low	0.009	33.29	-19.03	0.21	0.14	11.8	0.4	2.51	1.75	0.09	1
2002fk	low	0.007	32.54	-19.37	0.24	-0.09	9.8	0.3	1.84	0.07	0.08	2
2002ha	low	0.014	34.09	-19.37	0.14	-0.08	10.8	0.1	8.71	0.83	0.16	1
2002he	high	0.025	35.23	-18.98	0.09	0.02	12.4	0.1	21.17	0.0	0.1	1
2003cg	low	0.004	31.65	-15.81	0.32	1.22	10.9	0.2	1.6	5.43	0.23	1
2003fa	low	0.040	36.33	-19.72	0.07	-0.09	11.2	0.4	39.33	0.0	0.0	1
2003gn	low	0.034	35.90	-18.55	0.11	0.04	12.0	0.3	13.32	0.0 <sup>†</sup>	0.01	1
2003gt	low	0.015	34.26	-19.29	0.13	0.05	11.1	0.4	3.06	0.0 <sup>†</sup>	0.08	1
2004at	low	0.022	35.08	-19.40	0.09	-0.11	11.3	0.1	42.3	0.19	0.14	1
2004dt	high	0.020	34.64	-19.41	0.10	-0.004	13.3	0.3	45.09	0.46	0.21	1
2004ef	high	0.031	35.67	-18.80	0.10	0.08	12.8	0.4	6.69	0.9	0.27	1
2004eo	low	0.016	34.32	-19.22	0.14	0.02	10.8	0.4	18.03	0.0	0.2	1
2005cf	low	0.006	32.59	-19.28	0.25	0.03	10.1	0.1	17.25	0.3	0.06	1
2005de	low	0.015	34.37	-18.93	0.13	0.08	10.2	0.2	14.4	0.51	0.1	1
2005ki	low	0.019	34.84	-19.30	0.10	-0.01	11.1	0.2	29.6	0.3	0.09	1
2006cp	high	0.022	35.15	-19.23	0.11	-0.02	13.6	0.3	12.26	0.26	0.14	1
2006gr	low	0.035	35.92	-18.98	0.09	0.08	11.4	0.3	24.13	1.48	0.23	1
2006le	low	0.017	34.46	-19.50	0.11	-0.04	11.6	0.3	14.92	0.1	0.08	1
2007af	low	0.005	31.77	-18.61	0.28	0.05	10.6	0.1	6.01	0.31	0.08	2
2007le	high	0.007	32.41	-18.54	0.27	0.27	14.0	0.4	2.42	1.52	0.06	1
2007qe	high	0.024	35.10	-19.08	0.11	0.06	14.1	0.3	5.9	0.11	0.07	1
2008bf	low	0.024	35.33	-19.64	0.07	-0.15	11.5	0.2	25.73	0.08	0.15	1
2008ec	low	0.016	34.28	-18.72	0.13	0.15	10.5	0.1	4.71	0.61	0.12	1
2001V	low	0.015	34.36	-19.69	0.13	0.07	11.6	0.3	20.02	1.26	0.11	1
2005hk	low	0.013	33.75	-17.91	0.16	0.15	5.7	0.3	4.52	0.0 <sup>†</sup>	0.02	1
2006ax	low	0.017	34.57	-19.54	0.11	-0.03	10.5	0.1	20.34	0.0 <sup>†</sup>	0.1	1
2006lf	low	0.013	33.83	-19.62	0.16	-0.06	11.4	0.4	4.67	0.05 <sup>†</sup>	0.05	1
2007bd	high	0.026	35.42	-18.84	0.07	0.01	12.8	0.4	5.41	0.45	0.09	1
2007ci	low	0.018	34.71	-18.85	0.11	0.02	11.8	0.2	5.08	0.1	0.15	1
2005kc	low	0.015	34.15	-18.59	0.16	0.16	10.6	0.3	3.05	1.78	0.13	1
2007on	low	0.006	31.54	-18.49	0.23	0.11	11.3	0.3	8.98	0.02 <sup>†</sup>	0.0	3
2008gp	low	0.033	35.77	-19.29	0.08	0.004	11.3	0.4	11.74	0.0	0.14	1
2008hv	low	0.013	33.9	-19.11	0.13	0.05	10.9	0.2	10.01	0.0	0.19	1
2003W	high	0.020	34.87	-18.94	0.10	0.18	14.8	0.4	1.45	0.99	0.2	1
2003Y	faint	0.017	34.47	-16.74	0.14	0.81	9.8	0.3	7.03	0.0 <sup>†</sup>	0.08	1
2005M	low	0.025	35.28	-19.39	0.09	-0.05	10.6	0.2	3.35	0.25	0.13	1
2006X	high	0.005	31.04	-15.64	0.30	1.35	14.7	0.1	6.26	2.05	0.08	3
1991bg*	faint	0.003	31.40	-16.79	0.05	0.87	9.63	0.05	4.07	0.0 <sup>†</sup>	0.1	3
1999aa*	low	0.014	34.15	-19.57	0.03	-0.08	10.35	0.05	8.94	0.05	0.12	1
1998bu*	low	0.003	30.20	-18.17	0.02	0.32	10.75	0.2	3.43	0.45	0.1	3
1998bp*	low	0.010	33.65	-18.65	0.05	0.16	10.92	0.2	2.94	0.0	0.14	2
1998aq*	low	0.004	31.72	-19.46	0.02	-0.13	10.74	0.2	1.78	0.16	0.08	1
1996X*	low	0.007	32.24	-19.51	0.05	-0.10	11.17	0.22	8.85	0.0	0.12	1
1995D*	low	0.007	32.61	-19.65	0.06	-0.13	10.17	0.05	12.5	0.33	0.09	1
1994ae*	low	0.004	32.12	-19.28	0.06	-0.07	10.98	0.23	2.74	0.29	0.06	2
1990N*	low	0.003	31.81	-19.23	0.05	-0.003	9.38	0.22	4.45	0.0 <sup>†</sup>	0.1	2

**Table A.1.** continued.

SN Name	Type	$z$	$\mu$	$M_B$	$M_{\sigma,B}$	$B - V$	$v_{SiII}$	$\sigma v_{SiII}$	Offset [kpc]	EW Na I D [Å]	$\sigma_{NaID}$ [Å]	Ref.
1986G*	low	0.002	28.19	-16.58	0.08	0.82	10.47	0.05	4.08	0.34	0.01	3
2011fe*	low	0.001	29.18	-19.20	0.30	-0.02	10.58	0.05	4.67	0.07	0.05	2
2008Q*	low	0.008	32.69	-19.51	0.03	-0.07	11.42	0.2	24.69	0.0 <sup>†</sup>	0.04	2
2006D*	low	0.009	32.92	-18.96	0.04	0.029	10.42	0.05	2.22	0.0	0.05	2
2005ke*	faint	0.005	31.57	-16.79	0.05	0.72	8.97	0.2	5.76	0.0	0.1	1
2003hv*	low	0.006	31.89	-19.47	0.03	-0.07	10.91	0.2	6.56	0.0	0.1	1
2003du*	low	0.006	32.85	-19.46	0.03	-0.12	10.45	0.2	2.04	0.1	0.07	2
2002dp*	low	0.012	33.57	-19.15	0.03	0.09	11.48	0.2	10.68	0.7	0.14	1
2000E*	high	0.005	32.09	-20.58	0.24	-0.15	19.22	0.5	2.99	0.0 <sup>†</sup>	0.05	1
1999by*	faint	0.002	30.74	-17.26	0.03	0.43	10.0	0.2	5.99	0.0	0.2	4
1991T*	low	0.006	30.76	-19.24	0.02	0.13	10.0	0.4	6.12	1.3	0.14	5

**Notes.** The types of each SNe Ia studied in this work (low velocity, high velocity, or faint), the redshifts and Hubble flow distance moduli ( $\mu$ ) of their hosts, their peak  $B$ -band absolute magnitude ( $M_B$ ) and error ( $M_{\sigma,B}$ ), Si II velocities ( $v_{SiII}$ ) and errors ( $\sigma v_{SiII}$ ), physical offsets, and Na I D equivalent widths (EW) and errors ( $\sigma_{NaID}$ ). The references refer to the  $\mu$  measurements. All redshifts were acquired from NED. The  $B - V$  colors and Si II velocities were collected from Zheng et al. (2018) and Polin et al. (2021). We correct the  $M_B$  values in the Zheng et al. (2018) and Polin et al. (2021) samples using our collected  $\mu$ . We determine the all of the physical offsets and several of the Na I D EW and errors; the rest are from Wang et al. (2019).

\* Polin et al. (2021) SNe Ia sample (the rest are from Zheng et al. 2017)

<sup>†</sup> Na I D EW determined in this work (all others collected in Wang et al. 2019).

References: (1) Mould et al. 2000; (2) Riess et al. 2022; (3) Blakeslee et al. 2010; (4) Macri et al. 2001; (5) Saha et al. 2001

## Appendix B: Host Galaxy Photometry

Here, we record all host galaxy photometry used in the **Prospector** modeling.

**Table B.1.** Photometric Catalog

SN Name	R.A. (J2000)	Decl. (J2000)	Filter	$m_{AB}$
1998dh	348.6829	4.5344	U	10.45 ± 0.17
			B	12.0 ± 0.17
			V	11.53 ± 0.17
			R	11.45 ± 0.13
			I	10.58 ± 0.13
			J	10.29 ± 0.13
			H	10.22 ± 0.13
			K	10.17 ± 0.13
1998dm	21.5601	-6.0941	FUV	15.86 ± 0.13
			NUV	15.35 ± 0.13
			u	14.52 ± 0.13
			g	13.29 ± 0.13
			r	12.78 ± 0.13
			i	12.54 ± 0.13
			z	12.43 ± 0.13
			J	12.42 ± 0.13
			H	12.27 ± 0.13
			K	12.46 ± 0.13
			W1	14.77 ± 0.13
			W2	13.47 ± 0.13
1999cp	211.6454	-5.4531	FUV	13.78 ± 0.11
			NUV	13.46 ± 0.11
			U	13.53 ± 0.69
			B	12.74 ± 0.76
			V	12.44 ± 0.68
			J	12.43 ± 0.13
			H	12.25 ± 0.13
			K	12.46 ± 0.13
			W1	13.19 ± 0.13
			W2	13.72 ± 0.13
			W3	11.84 ± 0.13
			W4	11.05 ± 0.13
1999dq	38.5001	20.9768	FUV	16.34 ± 0.11
			NUV	15.88 ± 0.11
			U	13.7 ± 0.17
			B	12.69 ± 0.17
			V	12.36 ± 0.14

Table B.1. continued.

SN Name	R.A. (J2000)	Decl. (J2000)	Filter	$m_{AB}$
			J	$11.05 \pm 0.13$
			H	$10.85 \pm 0.13$
			K	$10.99 \pm 0.13$
			W1	$11.84 \pm 0.13$
			W2	$12.38 \pm 0.13$
			W3	$10.84 \pm 0.13$
			W4	$10.68 \pm 0.13$
1999gp	37.9169	39.3784	B	$13.72 \pm 0.27$
			J	$12.66 \pm 0.13$
			H	$12.43 \pm 0.13$
			K	$12.69 \pm 0.13$
			W1	$13.44 \pm 0.13$
			W2	$14.03 \pm 0.13$
			W3	$13.18 \pm 0.13$
2000cx	21.1988	9.5388	W4	$13.43 \pm 0.13$
			FUV	$18.43 \pm 0.11$
			NUV	$15.88 \pm 0.17$
			U	$12.3 \pm 0.13$
			B	$10.82 \pm 0.13$
			V	$10.02 \pm 0.13$
			r	$10.57 \pm 0.13$
			J	$9.03 \pm 0.13$
			H	$8.83 \pm 0.13$
			K	$9.05 \pm 0.13$
			W1	$10.64 \pm 0.13$
			W2	$11.33 \pm 0.13$
			W3	$12.02 \pm 0.13$
			W4	$12.53 \pm 0.13$
2000dn	346.2815	-3.2045	B	$14.65 \pm 0.15$
			J	$12.8 \pm 0.13$
			H	$12.58 \pm 0.13$
			K	$12.78 \pm 0.13$
			W1	$13.93 \pm 0.13$
			W2	$14.67 \pm 0.13$
			W3	$14.81 \pm 0.13$
W4	$15.15 \pm 0.9$			
2000dr	15.4274	-15.5678	FUV	$19.95 \pm 0.26$
			NUV	$18.32 \pm 0.11$
			B	$14.32 \pm 0.15$
			J	$11.82 \pm 0.13$
			H	$11.63 \pm 0.13$
			K	$11.82 \pm 0.13$
			W1	$13.16 \pm 0.13$
			W2	$13.9 \pm 0.13$
			W3	$14.76 \pm 0.13$
W4	$15.38 \pm 1.5$			
2000fa	108.8732	23.4262	B	$14.48 \pm 0.69$
			J	$13.58 \pm 0.13$
			H	$13.56 \pm 0.13$
			K	$13.22 \pm 0.13$
2001en	21.3364	34.025	FUV	$19.2 \pm 0.11$
			NUV	$18.2 \pm 0.11$
			U	$14.22 \pm 1.83$
			B	$13.13 \pm 1.74$
			V	$12.56 \pm 1.79$
			J	$11.68 \pm 0.13$
			H	$11.46 \pm 0.13$
			K	$11.61 \pm 0.13$
			W1	$13.9 \pm 0.13$
			W2	$14.43 \pm 0.13$
			W3	$13.15 \pm 0.13$
W4	$12.25 \pm 0.13$			
2001ep	74.2486	-4.7569	J	$12.58 \pm 0.13$
			H	$12.43 \pm 0.13$
			K	$12.61 \pm 0.13$
			W1	$14.4 \pm 0.13$
			W2	$15.05 \pm 0.13$



**Table B.1.** continued.

SN Name	R.A. (J2000)	Decl. (J2000)	Filter	$m_{AB}$			
2002bo	154.5235	21.8323	W3	$13.82 \pm 0.13$			
			W4	$13.07 \pm 0.13$			
			FUV	$17.67 \pm 0.11$			
			NUV	$16.08 \pm 0.11$			
			u	$13.19 \pm 0.13$			
			B	$11.85 \pm 0.13$			
			g	$11.54 \pm 0.13$			
			V	$11.08 \pm 0.13$			
			r	$10.74 \pm 0.13$			
			i	$10.3 \pm 0.13$			
			z	$9.99 \pm 2.09$			
			J	$9.52 \pm 0.13$			
			H	$9.25 \pm 0.13$			
			K	$9.43 \pm 0.13$			
			W1	$11.23 \pm 0.13$			
W2	$11.82 \pm 0.13$						
W3	$11.44 \pm 0.13$						
W4	$11.38 \pm 0.13$						
2002cr	211.6454	-5.4531	FUV	$13.66 \pm 0.13$			
			NUV	$13.36 \pm 0.13$			
			U	$13.53 \pm 0.69$			
			B	$12.74 \pm 0.68$			
			V	$12.44 \pm 0.68$			
			J	$12.43 \pm 0.13$			
			H	$12.25 \pm 0.13$			
			K	$12.46 \pm 0.13$			
			W1	$14.18 \pm 0.13$			
			W2	$14.67 \pm 0.13$			
			W3	$12.27 \pm 0.13$			
			W4	$11.05 \pm 0.13$			
			2002dj	198.2543	-19.5182	FUV	$18.46 \pm 0.13$
						NUV	$16.18 \pm 0.13$
						U	$12.51 \pm 0.16$
V	$10.51 \pm 0.17$						
R	$10.29 \pm 0.13$						
J	$9.56 \pm 0.13$						
H	$9.41 \pm 0.13$						
K	$9.59 \pm 0.13$						
W1	$11.38 \pm 0.13$						
W2	$11.97 \pm 0.13$						
W3	$12.51 \pm 0.13$						
W4	$12.1 \pm 0.13$						
2002dl	335.2213	33.2953				B	$14.4 \pm 0.27$
						I	$12.74 \pm 0.13$
						J	$12.18 \pm 0.13$
			H	$11.88 \pm 0.13$			
			K	$12.02 \pm 0.13$			
			W1	$13.92 \pm 0.13$			
			W2	$14.45 \pm 0.13$			
			W3	$13.42 \pm 0.13$			
			W4	$12.98 \pm 0.13$			
			2002eb	334.7762	24.5982	FUV	$18.25 \pm 0.13$
NUV	$17.9 \pm 0.13$						
B	$14.91 \pm 0.27$						
J	$13.54 \pm 0.13$						
H	$14.78 \pm 0.13$						
K	$14.81 \pm 0.13$						
W1	$14.57 \pm 0.13$						
W2	$14.7 \pm 0.13$						
W3	$13.0 \pm 0.13$						
W4	$11.84 \pm 0.13$						
2002er	247.878	7.9946	FUV	$19.86 \pm 0.31$			
			NUV	$18.5 \pm 0.13$			
			B	$14.43 \pm 0.14$			
			V	$13.94 \pm 0.14$			
			J	$12.3 \pm 0.13$			
			H	$12.79 \pm 0.13$			

Table B.1. continued.

SN Name	R.A. (J2000)	Decl. (J2000)	Filter	$m_{AB}$
			K	$12.31 \pm 0.13$
			W1	$13.36 \pm 0.13$
			W2	$13.75 \pm 0.13$
			W3	$11.4 \pm 0.13$
			W4	$10.26 \pm 0.13$
2002fk	50.5273	-15.4001	FUV	$15.6 \pm 0.13$
			NUV	$14.79 \pm 0.13$
			U	$12.38 \pm 0.17$
			B	$11.65 \pm 0.17$
			V	$11.42 \pm 0.17$
			J	$10.98 \pm 0.13$
			H	$10.83 \pm 0.13$
			K	$11.05 \pm 0.13$
			W1	$13.42 \pm 0.13$
			W2	$14.01 \pm 0.13$
			W3	$13.16 \pm 0.13$
			W4	$12.47 \pm 0.13$
2002ha	311.8294	0.3208	FUV	$17.75 \pm 0.13$
			NUV	$16.81 \pm 0.13$
			U	$13.69 \pm 0.39$
			B	$12.46 \pm 0.31$
			V	$11.86 \pm 0.59$
			R	$11.3 \pm 0.13$
			I	$10.85 \pm 0.13$
			J	$10.73 \pm 0.13$
			H	$10.56 \pm 0.13$
			K	$10.73 \pm 0.13$
			W1	$12.67 \pm 0.13$
			W2	$13.37 \pm 0.13$
			W3	$14.15 \pm 0.13$
			W4	$14.36 \pm 0.31$
2002he	125.0072	62.8306	J	$12.8 \pm 0.13$
			W2	$13.62 \pm 0.13$
			W3	$15.35 \pm 0.13$
2003cg	153.5627	3.4661	FUV	$16.78 \pm 0.13$
			NUV	$15.81 \pm 0.13$
			U	$11.96 \pm 0.18$
			B	$10.79 \pm 0.13$
			V	$10.14 \pm 0.13$
			I	$9.64 \pm 0.14$
			J	$11.26 \pm 0.13$
			H	$9.02 \pm 0.13$
			K	$9.21 \pm 0.13$
			W1	$11.07 \pm 0.13$
			W2	$11.56 \pm 0.13$
			W3	$10.54 \pm 0.13$
			W4	$10.15 \pm 0.13$
2003fa	266.0358	40.8573	B	$15.24 \pm 0.54$
			J	$13.64 \pm 0.13$
			H	$13.43 \pm 1.45$
			K	$13.51 \pm 0.13$
			W1	$14.55 \pm 0.13$
			W2	$15.03 \pm 0.13$
			W3	$13.0 \pm 0.22$
			W4	$12.16 \pm 0.13$
2003gn	338.4603	20.8053	FUV	$18.63 \pm \text{nan}$
			NUV	$18.07 \pm 0.13$
			B	$14.89 \pm 0.27$
			J	$16.0 \pm 0.15$
			H	$13.63 \pm 0.13$
			K	$15.85 \pm 0.13$
			W1	$15.12 \pm 0.13$
			W2	$15.72 \pm 0.13$
			W3	$14.25 \pm 0.59$
			W4	$13.78 \pm 0.13$
2003gt	308.245	9.8744	FUV	$18.24 \pm 0.15$
			NUV	$17.57 \pm 0.13$

**Table B.1.** continued.

SN Name	R.A. (J2000)	Decl. (J2000)	Filter	$m_{AB}$
			U	$14.08 \pm 0.26$
			B	$13.05 \pm 0.23$
			V	$12.46 \pm 0.24$
			J	$13.58 \pm 0.13$
			H	$13.26 \pm 0.13$
			K	$13.41 \pm 0.13$
			W1	$13.71 \pm 0.13$
			W2	$14.3 \pm 0.13$
			W3	$13.01 \pm 0.13$
			W4	$12.09 \pm 0.13$
2004at	164.6954	59.4868	u	$16.88 \pm 0.13$
			g	$15.87 \pm 0.13$
			r	$15.48 \pm 0.13$
			i	$15.31 \pm 0.13$
			z	$15.12 \pm 0.13$
			J	$16.39 \pm 0.18$
			K	$16.59 \pm 0.16$
2004dt	30.5514	-0.1006	FUV	$19.37 \pm 0.13$
			NUV	$18.31 \pm 0.13$
			u	$15.37 \pm 0.13$
			B	$13.83 \pm 0.64$
			g	$13.71 \pm 0.13$
			V	$12.89 \pm 0.25$
			r	$12.95 \pm 0.13$
			i	$12.57 \pm 0.13$
			z	$12.33 \pm 0.13$
			J	$12.25 \pm 0.13$
			H	$12.07 \pm 0.13$
			K	$12.26 \pm 0.13$
			W1	$13.75 \pm 0.13$
			W2	$14.47 \pm 0.13$
			W3	$14.29 \pm 0.13$
			W4	$14.14 \pm 0.16$
2004ef	340.5438	19.997	NUV	$18.5 \pm 0.13$
			B	$14.38 \pm 0.5$
			J	$14.8 \pm 0.13$
			H	$14.67 \pm 0.13$
			K	$14.94 \pm 0.13$
			W1	$14.82 \pm 0.13$
			W2	$15.57 \pm 0.13$
			W3	$16.31 \pm 0.24$
2004eo	308.2092	9.9264	U	$13.79 \pm 0.22$
			B	$12.59 \pm 0.21$
			V	$11.92 \pm 0.21$
			J	$10.72 \pm 0.13$
			H	$10.47 \pm 0.13$
			K	$10.6 \pm 0.13$
			W1	$12.24 \pm 0.13$
			W2	$12.82 \pm 0.13$
			W3	$12.18 \pm 0.13$
			W4	$11.86 \pm 0.13$
2005cf	230.3857	-7.3772	FUV	$14.66 \pm 0.13$
			NUV	$14.39 \pm 0.13$
			B	$13.26 \pm 2.11$
			R	$13.67 \pm \text{nan}$
			I	$13.7 \pm 4.31$
			J	$12.56 \pm 0.13$
			H	$12.39 \pm 0.13$
			K	$12.71 \pm 0.13$
			W1	$14.07 \pm 0.13$
			W2	$14.56 \pm 0.13$
			W3	$12.19 \pm 0.13$
			W4	$10.56 \pm 0.13$
2005de	270.6036	36.0404	B	$14.48 \pm 0.29$
			J	$12.44 \pm 0.13$
			H	$12.22 \pm 0.13$
			K	$12.35 \pm 0.13$

Table B.1. continued.

SN Name	R.A. (J2000)	Decl. (J2000)	Filter	$m_{AB}$
2005ki	160.1182	9.1826	u	15.15 ± 0.13
			g	13.27 ± 0.13
			r	12.47 ± 0.13
			i	12.06 ± 0.13
			z	11.81 ± 0.13
			J	11.4 ± 0.13
			H	11.23 ± 0.13
			K	11.39 ± 0.13
			W1	13.07 ± 0.13
			W2	13.75 ± 0.13
2006cp	184.8058	22.4315	u	15.45 ± 0.13
			g	14.33 ± 0.13
			r	13.84 ± 0.13
			i	13.62 ± 0.13
			z	13.5 ± 0.13
			J	13.13 ± 0.17
			H	12.38 ± 0.21
			K	12.12 ± 0.28
2006gr	338.1021	30.8356	B	14.49 ± 0.27
			J	14.03 ± 0.13
			H	13.76 ± 0.13
			K	13.94 ± 0.13
			W1	14.1 ± 0.13
			W2	14.66 ± 0.13
			W3	12.95 ± 0.13
			W4	12.5 ± 0.13
2006le	75.1821	62.244	B	12.64 ± 0.32
			J	11.07 ± 0.13
			H	10.85 ± 0.13
			K	11.07 ± 0.13
			W1	13.05 ± 0.13
			W2	13.61 ± 0.13
			W3	11.99 ± 0.13
			W4	11.51 ± 0.13
2007af	215.599	-0.3877	NUV	15.12 ± 0.13
			u	14.71 ± 0.13
			B	14.25 ± 0.13
			g	13.64 ± 0.13
			r	13.02 ± 0.13
			i	12.65 ± 0.13
			z	12.57 ± 0.13
2007le	354.7027	-6.5179	FUV	16.7 ± 0.13
			NUV	15.86 ± 0.13
			U	12.68 ± 0.21
			B	11.93 ± 0.21
			V	11.51 ± 0.21
			J	10.66 ± 0.13
			H	10.49 ± 0.13
			K	10.7 ± 0.13
			W1	13.29 ± 0.13
			W2	13.85 ± 0.28
			W3	11.95 ± 0.13
			W4	11.27 ± 0.13
2007qe	358.5504	27.409	FUV	20.16 ± 0.28
			NUV	21.14 ± 0.13
			u	18.52 ± 0.13
			g	17.39 ± 0.13
			r	16.92 ± 0.13
			i	16.68 ± 0.13
			z	16.72 ± 0.13
			J	17.62 ± 0.29
			W1	17.76 ± 0.13
			W2	19.03 ± 0.77
W3	14.59 ± 0.13			
2008bf	181.0068	20.2724	B	13.57 ± 0.21
			g	13.73 ± 0.13
			V	13.0 ± 0.21

**Table B.1.** continued.

SN Name	R.A. (J2000)	Decl. (J2000)	Filter	$m_{AB}$
			r	$12.92 \pm 0.13$
			i	$12.5 \pm 0.13$
			z	$12.17 \pm 0.13$
			J	$12.79 \pm 0.13$
			H	$12.58 \pm 0.13$
			K	$12.72 \pm 0.13$
			W1	$13.08 \pm 0.13$
			W2	$13.76 \pm 0.13$
			W3	$13.85 \pm 0.13$
2008ec	345.8151	8.874	W4	$13.53 \pm 0.14$
			FUV	$16.25 \pm 0.13$
			NUV	$15.47 \pm 0.13$
			U	$13.06 \pm 0.32$
			B	$12.58 \pm 0.32$
			V	$12.15 \pm 0.33$
			J	$11.14 \pm 0.13$
			H	$10.83 \pm 0.13$
			K	$10.83 \pm 0.13$
2001V	179.359	25.2331	W1	$11.1 \pm 0.13$
			W2	$10.95 \pm 0.13$
			W3	$8.88 \pm 0.13$
			FUV	$18.18 \pm 0.13$
			NUV	$17.73 \pm 0.13$
			u	$16.74 \pm 0.13$
			B	$15.47 \pm 0.26$
			g	$15.56 \pm 0.13$
			r	$15.05 \pm 0.13$
2005hk	6.9572	-1.1999	i	$14.81 \pm 0.13$
			z	$14.68 \pm 0.13$
			J	$14.93 \pm 0.13$
			H	$14.8 \pm 0.13$
			K	$15.05 \pm 0.13$
			W1	$16.11 \pm 0.13$
			W2	$16.56 \pm 0.13$
			W3	$14.84 \pm 0.13$
			W4	$14.11 \pm 0.19$
2006ax	170.999	-12.2964	FUV	$16.48 \pm 0.13$
			NUV	$16.26 \pm 0.13$
			u	$15.91 \pm 0.13$
			B	$14.77 \pm 0.4$
			g	$14.8 \pm 0.13$
			r	$14.35 \pm 0.13$
			i	$14.14 \pm 0.13$
			z	$14.16 \pm 0.13$
			J	$15.07 \pm 0.13$
2006lf	69.618	44.0371	H	$14.81 \pm 0.13$
			K	$15.29 \pm 0.25$
			W1	$16.49 \pm 0.13$
			W2	$17.08 \pm 0.13$
			W3	$15.88 \pm 0.13$
			W4	$14.88 \pm 0.46$
			r	$15.19 \pm 0.13$
			W1	$14.73 \pm 0.13$
			W2	$15.47 \pm 0.13$
2007bd	127.887	-1.1977	W3	$15.48 \pm 0.13$
			W4	$14.27 \pm 0.27$
			I	$11.2 \pm 0.13$
			J	$11.23 \pm 0.13$
			H	$11.05 \pm 0.13$
			K	$11.27 \pm 0.13$
			W1	$13.53 \pm 0.13$
			W2	$14.09 \pm 0.13$
			W3	$13.03 \pm 0.13$
2007bd	127.887	-1.1977	W4	$11.9 \pm 0.13$
			B	$14.3 \pm 0.27$
			J	$13.11 \pm 0.13$
			H	$12.92 \pm 0.13$

Table B.1. continued.

SN Name	R.A. (J2000)	Decl. (J2000)	Filter	$m_{AB}$
			K	$13.07 \pm 0.13$
			W1	$14.77 \pm 0.13$
			W2	$15.53 \pm 0.13$
			W3	$15.76 \pm 0.13$
			W4	$14.52 \pm 0.36$
2007ci	176.4421	19.7739	FUV	$19.83 \pm 0.4$
			NUV	$18.62 \pm 0.13$
			U	$14.9 \pm 0.27$
			B	$13.58 \pm 0.21$
			V	$12.78 \pm 0.21$
			R	$13.27 \pm 0.13$
			J	$11.79 \pm 0.13$
			H	$11.57 \pm 0.13$
			K	$11.82 \pm 0.13$
			W1	$13.3 \pm 0.13$
			W2	$14.0 \pm 0.13$
			W3	$15.37 \pm 0.13$
			W4	$15.15 \pm 0.7$
2005kc	338.528	5.5699	NUV	$17.07 \pm 0.13$
			B	$12.71 \pm 0.29$
			V	$12.42 \pm 0.14$
			J	$10.82 \pm 0.13$
			H	$10.6 \pm 0.13$
			K	$10.8 \pm 0.13$
2007on	54.7145	-35.5939	FUV	$16.65 \pm 0.13$
			NUV	$15.65 \pm 0.13$
			U	$12.24 \pm 0.17$
			B	$10.76 \pm 0.17$
			V	$9.97 \pm 0.17$
			r	$10.36 \pm 0.13$
			J	$8.78 \pm 0.13$
			H	$8.57 \pm 0.13$
			K	$8.77 \pm 0.13$
			W1	$10.71 \pm 0.13$
			W2	$11.4 \pm 0.13$
			W3	$12.11 \pm 0.13$
			W4	$13.06 \pm 0.13$
2008gp	50.762	1.371	B	$13.97 \pm 0.32$
			J	$14.23 \pm 0.13$
			H	$14.16 \pm 0.13$
			K	$14.5 \pm 0.13$
			W1	$14.47 \pm 0.13$
			W2	$15.1 \pm 0.13$
			W3	$13.96 \pm 0.13$
			W4	$13.3 \pm 0.13$
2008hv	136.9027	3.3929	B	$12.79 \pm 0.21$
			g	$12.87 \pm 0.13$
			r	$12.21 \pm 0.13$
			I	$11.83 \pm 0.13$
			z	$11.99 \pm 0.13$
			J	$11.13 \pm 0.13$
			H	$10.95 \pm 0.13$
			K	$11.15 \pm 0.13$
			W1	$13.02 \pm 0.13$
			W2	$13.71 \pm 0.13$
			W3	$14.94 \pm 0.13$
			W4	$15.25 \pm 0.66$
2003W	146.7063	16.0429	NUV	$17.17 \pm 0.13$
			u	$12.83 \pm 0.13$
			B	$13.85 \pm 0.32$
			g	$13.77 \pm 0.13$
			r	$13.13 \pm 0.13$
			i	$12.72 \pm 0.13$
			z	$12.52 \pm 0.13$
			J	$9.65 \pm 0.13$
			H	$12.17 \pm 0.13$
			K	$12.32 \pm 0.13$

Table B.1. continued.

SN Name	R.A. (J2000)	Decl. (J2000)	Filter	$m_{AB}$			
2003Y	133.6455	57.1667	g	$13.6 \pm 0.13$			
			r	$12.82 \pm 0.13$			
			i	$12.41 \pm 0.13$			
			z	$12.12 \pm 0.13$			
			J	$11.94 \pm 0.13$			
			H	$11.72 \pm 0.13$			
			K	$11.91 \pm 0.13$			
			W1	$13.36 \pm 0.13$			
			W2	$14.06 \pm 0.13$			
			W3	$15.06 \pm 0.13$			
2005M	144.3858	23.025	u	$15.67 \pm 0.13$			
			B	$14.83 \pm 0.32$			
			g	$14.88 \pm 0.13$			
			r	$14.5 \pm 0.13$			
			i	$14.36 \pm 0.13$			
			z	$14.21 \pm 0.13$			
			J	$16.39 \pm 0.19$			
			H	$15.39 \pm 0.13$			
			K	$15.58 \pm 0.13$			
			2006X	185.7285	15.8218	FUV	$14.12 \pm 0.14$
NUV	$13.22 \pm 0.13$						
U	$10.69 \pm 0.13$						
B	$9.78 \pm 0.13$						
g	$10.74 \pm 0.13$						
V	$9.28 \pm 0.13$						
r	$10.27 \pm 0.13$						
i	$12.44 \pm 2.09$						
z	$9.75 \pm 0.13$						
J	$9.36 \pm 0.13$						
H	$9.2 \pm 0.13$						
K	$9.38 \pm 0.13$						
1991bg	186.2656	12.887				FUV	$17.72 \pm 0.13$
						NUV	$15.98 \pm 0.13$
			U	$11.2 \pm 0.13$			
			B	$9.97 \pm 0.13$			
			g	$9.59 \pm 0.13$			
			V	$9.0 \pm 0.13$			
			r	$8.82 \pm 0.13$			
			I	$9.45 \pm 0.13$			
			z	$8.2 \pm 0.13$			
			J	$8.12 \pm 0.13$			
			H	$7.94 \pm 0.13$			
			K	$8.17 \pm 0.13$			
			1999aa	126.9303	21.5166	FUV	$15.41 \pm 0.13$
						NUV	$17.02 \pm 0.13$
u	$15.42 \pm 0.13$						
U	$13.59 \pm 0.2$						
B	$12.44 \pm 0.21$						
g	$13.88 \pm 0.13$						
V	$11.93 \pm 0.21$						
r	$13.06 \pm 0.13$						
i	$12.67 \pm 0.13$						
z	$12.34 \pm 0.13$						
J	$11.75 \pm 0.13$						
H	$11.64 \pm 0.13$						
K	$11.81 \pm 0.13$						
W1	$13.49 \pm 0.13$						
W2	$14.2 \pm 0.13$						
W3	$12.95 \pm 0.13$						
W4	$12.5 \pm 0.13$						
1998bu	161.6906	11.8199	FUV	$16.15 \pm 0.13$			
			NUV	$15.01 \pm 0.13$			
			U	$11.07 \pm 0.17$			
			B	$9.85 \pm 0.17$			
			V	$9.18 \pm 0.17$			
			r	$10.09 \pm 0.13$			
			i	$9.68 \pm 0.13$			

Table B.1. continued.

SN Name	R.A. (J2000)	Decl. (J2000)	Filter	$m_{AB}$
			z	$9.19 \pm 0.13$
			J	$8.62 \pm 0.13$
			H	$8.01 \pm 0.13$
			K	$8.24 \pm 0.13$
1998bp	268.7115	18.3269	B	$12.7 \pm 0.25$
			V	$12.83 \pm 0.14$
			J	$11.34 \pm 0.13$
			H	$11.04 \pm 0.13$
			K	$11.39 \pm 0.13$
			W1	$12.89 \pm 0.13$
			W2	$13.57 \pm 0.13$
1998aq	179.1172	55.1252	u	$13.37 \pm 0.13$
			B	$11.56 \pm 0.23$
			g	$12.16 \pm 0.13$
			V	$11.55 \pm 0.13$
			r	$11.56 \pm 0.13$
			i	$11.28 \pm 0.13$
			z	$11.11 \pm 0.13$
			J	$10.73 \pm 0.13$
			H	$10.54 \pm 0.13$
			K	$10.76 \pm 0.13$
			W1	$13.01 \pm 0.13$
			W2	$13.38 \pm 0.13$
			W3	$11.23 \pm 0.13$
			W4	$9.72 \pm 0.13$
1996X	199.5211	-26.8372	V	$10.17 \pm 0.17$
			r	$10.73 \pm 0.13$
			J	$9.13 \pm 0.13$
			H	$8.96 \pm 0.13$
			K	$9.19 \pm 0.13$
			W1	$11.32 \pm 0.13$
			W2	$11.97 \pm 0.13$
			W3	$13.06 \pm 0.13$
			W4	$13.2 \pm 0.13$
1995D	145.221	5.1658	B	$12.58 \pm 0.17$
			g	$12.8 \pm 0.13$
			V	$11.77 \pm 0.17$
			i	$11.51 \pm 0.13$
			z	$11.2 \pm 0.13$
			J	$10.64 \pm 0.13$
			H	$10.42 \pm 0.13$
			K	$10.62 \pm 0.13$
			W1	$12.56 \pm 0.13$
			W2	$13.24 \pm 0.13$
			W3	$14.07 \pm 0.13$
			W4	$13.85 \pm 0.15$
1994ae	161.7669	17.2736	FUV	$14.27 \pm 0.13$
			NUV	$15.6 \pm 0.13$
			u	$13.92 \pm 0.13$
			B	$11.99 \pm 0.21$
			g	$12.68 \pm 0.13$
			r	$12.07 \pm 0.13$
			i	$11.74 \pm 0.13$
			I	$11.46 \pm 0.13$
			z	$11.48 \pm 0.13$
			J	$11.34 \pm 0.13$
			H	$11.16 \pm 0.13$
			K	$11.26 \pm 0.13$
			W1	$13.33 \pm 0.13$
			W2	$13.87 \pm 0.13$
			W3	$12.06 \pm 0.13$
			W4	$11.31 \pm 0.13$
1990N	190.7183	13.2574	FUV	$14.37 \pm 0.13$
			NUV	$14.05 \pm 0.13$
			u	$12.88 \pm 0.13$
			U	$12.96 \pm 0.13$
			B	$11.97 \pm 0.13$



**Table B.1.** continued.

SN Name	R.A. (J2000)	Decl. (J2000)	Filter	$m_{AB}$
			g	$11.66 \pm 0.13$
			V	$11.47 \pm 0.13$
			I	$10.78 \pm 0.13$
			J	$10.65 \pm 0.13$
			H	$10.51 \pm 0.13$
			K	$10.75 \pm 0.13$
			W1	$12.76 \pm 0.34$
			W2	$13.32 \pm 0.13$
			W3	$13.52 \pm 0.13$
			W4	$12.99 \pm 0.13$
1986G	201.3651	-43.0191	FUV	$13.36 \pm 0.13$
			NUV	$11.69 \pm 0.13$
			B	$7.25 \pm 0.13$
			V	$6.49 \pm 0.13$
			R	$6.22 \pm 0.13$
			J	$5.84 \pm 0.13$
			H	$5.63 \pm 0.13$
			K	$5.83 \pm 0.13$
			W1	$8.39 \pm 0.13$
			W2	$8.5 \pm 0.13$
			W3	$7.78 \pm 0.13$
			W4	$6.87 \pm 0.13$
2011fe	210.8023	54.349	FUV	$12.19 \pm 0.13$
			NUV	$11.51 \pm 0.13$
			B	$3.11 \pm 0.13$
			V	$7.83 \pm 0.13$
			R	$7.74 \pm 0.13$
			J	$7.46 \pm 0.13$
			H	$7.23 \pm 0.13$
			K	$7.42 \pm 0.13$
			W1	$7.88 \pm 0.13$
			W2	$8.36 \pm 0.13$
			W3	$6.59 \pm 0.13$
			W4	$6.61 \pm 0.13$
2008Q	21.1988	9.5388	FUV	$18.03 \pm 0.13$
			NUV	$17.11 \pm 0.13$
			V	$10.02 \pm 0.13$
			R	$9.99 \pm 0.13$
			J	$9.03 \pm 0.13$
			H	$8.83 \pm 0.13$
			K	$9.05 \pm 0.13$
			W1	$11.45 \pm 0.13$
			W2	$12.09 \pm 0.13$
			W3	$12.49 \pm 0.13$
			W4	$12.7 \pm 0.13$
2006D	193.1446	9.7767	FUV	$16.09 \pm 0.13$
			NUV	$15.7 \pm 0.13$
			J	$12.53 \pm 0.13$
			H	$12.34 \pm 0.13$
			K	$12.48 \pm 0.13$
			W1	$13.24 \pm 0.13$
			W2	$13.64 \pm 0.13$
			W3	$11.16 \pm 0.13$
			W4	$9.55 \pm 0.13$
2005ke	53.7556	-24.9332	FUV	$14.27 \pm 0.13$
			NUV	$13.94 \pm 0.13$
			U	$12.69 \pm 0.14$
			B	$11.31 \pm 0.14$
			V	$10.6 \pm 0.14$
			R	$10.1 \pm 0.13$
			J	$9.5 \pm 0.13$
			H	$9.32 \pm 0.13$
			K	$9.52 \pm 0.13$
			W1	$12.34 \pm 0.13$
			W2	$12.93 \pm 0.13$
			W3	$13.68 \pm 0.13$
			W4	$13.24 \pm 0.13$

Table B.1. continued.

SN Name	R.A. (J2000)	Decl. (J2000)	Filter	$m_{AB}$
2003hv	46.0332	-26.0696	U	12.88 ± 0.19
			B	11.44 ± 0.19
			V	10.68 ± 0.19
			R	10.5 ± 0.13
			J	9.53 ± 0.13
			H	9.33 ± 0.13
			K	9.57 ± 0.13
			W1	11.53 ± 0.13
			W2	12.2 ± 0.13
			W3	13.5 ± 0.13
W4	13.68 ± 0.13			
2003du	218.6542	59.3378	u	16.16 ± 0.13
			B	14.58 ± 0.21
			g	14.86 ± 0.13
			V	14.24 ± 0.22
			r	14.51 ± 0.13
			i	14.55 ± 0.13
			z	14.32 ± 0.13
2002dp	352.1162	22.4212	FUV	14.68 ± 0.11
			NUV	14.25 ± 0.35
			B	12.06 ± 0.23
			V	11.69 ± 0.25
			J	11.17 ± 0.13
			H	11.01 ± 0.13
			K	11.16 ± 0.13
			W1	13.36 ± 0.13
			W2	13.78 ± 0.13
			W3	11.44 ± 0.13
W4	9.97 ± 0.13			
2002cs	281.7399	45.7057	NUV	18.95 ± 0.13
			U	14.03 ± 0.22
			B	12.67 ± 0.21
			V	11.94 ± 0.21
			r	13.24 ± 0.13
			J	11.1 ± 0.13
			H	10.86 ± 0.13
			K	11.11 ± 0.13
			W1	12.77 ± 0.13
			W2	13.44 ± 0.13
W3	14.52 ± 0.13			
W4	14.66 ± 0.21			
2000E	309.3087	65.1056	FUV	14.47 ± 0.13
			NUV	13.39 ± 0.13
			B	9.82 ± 0.21
			V	9.4 ± 0.22
			J	9.01 ± 0.13
			H	8.8 ± 0.13
			K	9.06 ± 0.13
			W1	11.65 ± 0.13
			W2	12.1 ± 0.13
			W3	10.32 ± 0.13
W4	9.05 ± 0.13			
1999by	140.511	50.9765	FUV	15.9 ± 0.13
			NUV	14.94 ± 0.13
			U	11.12 ± 0.13
			B	9.86 ± 0.13
			g	9.74 ± 0.9
			V	9.16 ± 0.13
			r	9.0 ± 0.75
			I	8.41 ± 0.13
			J	7.97 ± 0.13
			H	7.74 ± 0.13
			K	7.98 ± 0.13
			W1	10.95 ± 0.13
			W2	11.63 ± 0.13
W3	12.69 ± 0.13			
W4	12.74 ± 0.13			

**Table B.1.** continued.

SN Name	R.A. (J2000)	Decl. (J2000)	Filter	$m_{AB}$
1991T	188.5351	2.6537	FUV	$14.95 \pm 0.13$
			NUV	$14.27 \pm 0.13$
			u	$12.56 \pm 0.13$
			U	$12.25 \pm 0.17$
			B	$11.12 \pm 0.13$
			g	$10.89 \pm 0.13$
			V	$10.45 \pm 0.13$
			r	$10.14 \pm 0.13$
			i	$9.69 \pm 0.13$
			z	$9.36 \pm 0.13$
			J	$9.01 \pm 0.13$
			H	$8.71 \pm 0.13$
			K	$8.86 \pm 0.13$

**Notes.** The SNe names and the respective coordinates (R.A. and Decl.), filters, and photometric magnitudes of their host galaxies. All photometry is from NED and corrected for Galactic extinction in the direction in the direction of the SNe.

### Appendix C: Host Galaxy Properties

Here, we record all stellar population properties of the host galaxies of SNe Ia studied in this work.

**Table C.1.** Host Data

SN Name	Type	$z$	$t_m$	$\log(M_*/M_\odot)$	SFR [ $M_\odot/\text{yr}$ ]	$\log(Z_*/Z_\odot)$	$A_V$ [mag]
1998dh	low	0.009	$3.25^{+1.97}_{-1.84}$	$10.52^{+0.15}_{-0.21}$	$9.11^{+7.05}_{-6.37}$	$-0.0^{+0.12}_{-0.13}$	$1.63^{+0.69}_{-0.72}$
1998dm	low	0.0065	$0.72^{+0.02}_{-0.03}$	$8.93^{+0.01}_{-0.01}$	$0.02^{+0.01}_{-0.0}$	$-1.19^{+0.01}_{-0.01}$	$0.09^{+0.03}_{-0.03}$
1999cp	low	0.0095	$0.54^{+0.23}_{-0.13}$	$9.31^{+0.1}_{-0.07}$	$4.3^{+0.32}_{-0.4}$	$-0.54^{+0.14}_{-0.22}$	$0.33^{+0.12}_{-0.11}$
1999dq	low	0.0143	$4.72^{+1.67}_{-1.15}$	$10.68^{+0.06}_{-0.06}$	$4.24^{+0.56}_{-0.66}$	$-0.34^{+0.1}_{-0.11}$	$1.44^{+0.17}_{-0.19}$
1999gp	low	0.0267	$3.05^{+2.02}_{-1.24}$	$10.47^{+0.11}_{-0.1}$	$2.55^{+1.89}_{-1.57}$	$-0.26^{+0.1}_{-0.12}$	$0.16^{+0.17}_{-0.07}$
2000cx	low	0.008	$6.87^{+0.75}_{-0.72}$	$10.86^{+0.03}_{-0.03}$	$0.01^{+0.0}_{-0.0}$	$-0.49^{+0.05}_{-0.05}$	$0.08^{+0.03}_{-0.02}$
2000dn	low	0.0321	$2.98^{+0.98}_{-0.62}$	$10.56^{+0.08}_{-0.07}$	$0.0^{+0.06}_{-0.0}$	$-0.58^{+0.09}_{-0.11}$	$0.21^{+0.14}_{-0.08}$
2000dr	low	0.0188	$8.19^{+1.29}_{-1.22}$	$10.66^{+0.04}_{-0.05}$	$0.02^{+0.01}_{-0.01}$	$-0.44^{+0.08}_{-0.07}$	$0.11^{+0.06}_{-0.04}$
2000fa	low	0.0213	$0.03^{+0.03}_{-0.02}$	$9.27^{+0.17}_{-0.17}$	$57.27^{+16.08}_{-14.02}$	$-1.01^{+0.07}_{-0.12}$	$3.12^{+0.59}_{-0.48}$
2001en	high	0.0159	$4.61^{+1.33}_{-1.0}$	$10.09^{+0.05}_{-0.05}$	$1.04^{+0.12}_{-0.11}$	$-0.96^{+0.12}_{-0.09}$	$1.77^{+0.2}_{-0.21}$
2001ep	low	0.0131	$0.61^{+0.06}_{-0.05}$	$9.49^{+0.02}_{-0.02}$	$0.23^{+0.11}_{-0.07}$	$-1.17^{+0.04}_{-0.02}$	$0.35^{+0.12}_{-0.09}$
2002bo	high	0.0044	$7.3^{+1.41}_{-0.88}$	$10.43^{+0.05}_{-0.04}$	$0.12^{+0.02}_{-0.02}$	$-0.76^{+0.06}_{-0.06}$	$0.47^{+0.07}_{-0.07}$
2002cr	low	0.0095	$0.19^{+0.02}_{-0.03}$	$9.06^{+0.05}_{-0.05}$	$2.62^{+0.19}_{-0.19}$	$-1.04^{+0.07}_{-0.1}$	$0.18^{+0.04}_{-0.03}$
2002dj	high	0.0094	$3.28^{+0.09}_{-0.18}$	$10.9^{+0.01}_{-0.03}$	$0.0^{+0.15}_{-0.0}$	$-1.0^{+0.0}_{-0.0}$	$0.19^{+0.03}_{-0.03}$
2002dl	low	0.0163	$1.56^{+0.75}_{-0.33}$	$9.91^{+0.09}_{-0.06}$	$0.26^{+0.16}_{-0.13}$	$-1.17^{+0.05}_{-0.02}$	$0.69^{+0.16}_{-0.14}$
2002eb	low	0.0275	$0.84^{+0.16}_{-0.17}$	$9.65^{+0.04}_{-0.05}$	$6.04^{+0.35}_{-0.33}$	$-1.1^{+0.1}_{-0.06}$	$2.6^{+0.28}_{-0.23}$
2002er	low	0.0085	$0.75^{+0.26}_{-0.32}$	$9.33^{+0.05}_{-0.07}$	$2.79^{+0.22}_{-0.29}$	$-1.02^{+0.15}_{-0.11}$	$2.57^{+0.33}_{-0.3}$
2002fk	low	0.0071	$0.69^{+0.02}_{-0.02}$	$9.39^{+0.01}_{-0.01}$	$0.08^{+0.01}_{-0.01}$	$-1.18^{+0.03}_{-0.01}$	$0.3^{+0.04}_{-0.04}$
2002ha	low	0.014	$9.86^{+0.56}_{-1.0}$	$10.8^{+0.02}_{-0.04}$	$0.08^{+0.02}_{-0.01}$	$-0.84^{+0.03}_{-0.07}$	$0.07^{+0.03}_{-0.03}$
2002he	high	0.0246	$12.12^{+0.6}_{-0.84}$	$10.89^{+0.02}_{-0.03}$	$0.0^{+0.0}_{-0.0}$	$0.02^{+0.06}_{-0.06}$	$0.01^{+0.03}_{-0.01}$
2003cg	low	0.0041	$0.74^{+0.06}_{-0.05}$	$9.83^{+0.02}_{-0.02}$	$0.32^{+0.06}_{-0.05}$	$0.26^{+0.03}_{-0.05}$	$2.32^{+0.27}_{-0.29}$
2003fa	low	0.0404	$1.02^{+0.3}_{-0.32}$	$10.08^{+0.06}_{-0.06}$	$13.35^{+1.19}_{-1.16}$	$-0.56^{+0.1}_{-0.12}$	$1.2^{+0.32}_{-0.27}$
2003gn	low	0.0344	$1.89^{+0.5}_{-0.51}$	$9.49^{+0.06}_{-0.06}$	$1.9^{+0.22}_{-0.13}$	$0.24^{+0.04}_{-0.07}$	$1.01^{+0.12}_{-0.08}$
2003gt	low	0.0152	$1.66^{+1.73}_{-0.86}$	$9.67^{+0.11}_{-0.06}$	$1.49^{+0.34}_{-0.42}$	$-0.28^{+0.27}_{-0.28}$	$2.39^{+0.57}_{-0.39}$
2004at	low	0.0224	$0.59^{+0.05}_{-0.06}$	$8.99^{+0.02}_{-0.03}$	$0.09^{+0.06}_{-0.03}$	$-1.16^{+0.05}_{-0.03}$	$0.1^{+0.12}_{-0.07}$
2004dt	high	0.0198	$9.7^{+0.47}_{-0.9}$	$10.61^{+0.02}_{-0.03}$	$0.1^{+0.03}_{-0.03}$	$-0.98^{+0.06}_{-0.04}$	$0.29^{+0.07}_{-0.07}$
2004ef	high	0.031	$1.43^{+0.33}_{-0.27}$	$9.66^{+0.04}_{-0.02}$	$0.25^{+0.06}_{-0.05}$	$0.26^{+0.02}_{-0.04}$	$0.14^{+0.12}_{-0.09}$
2004eo	low	0.0156	$2.19^{+1.2}_{-0.54}$	$10.56^{+0.09}_{-0.06}$	$1.16^{+0.64}_{-0.58}$	$-0.75^{+0.12}_{-0.13}$	$0.53^{+0.11}_{-0.13}$
2005cf	low	0.0064	$0.26^{+0.03}_{-0.03}$	$8.76^{+0.05}_{-0.07}$	$0.76^{+0.09}_{-0.07}$	$-1.05^{+0.12}_{-0.1}$	$0.54^{+0.1}_{-0.1}$
2005de	low	0.0153	$4.08^{+3.01}_{-2.36}$	$10.19^{+0.22}_{-0.21}$	$2.08^{+0.97}_{-2.08}$	$-0.04^{+0.2}_{-0.24}$	$1.36^{+0.92}_{-0.89}$
2005ki	low	0.0195	$2.18^{+0.8}_{-0.53}$	$10.57^{+0.08}_{-0.08}$	$0.0^{+0.02}_{-0.0}$	$-0.99^{+0.11}_{-0.12}$	$0.85^{+0.21}_{-0.14}$
2006cp	high	0.0223	$1.95^{+1.88}_{-1.1}$	$10.07^{+0.15}_{-0.15}$	$6.28^{+5.29}_{-2.29}$	$-0.03^{+0.22}_{-0.35}$	$1.18^{+0.72}_{-0.5}$
2006gr	low	0.0347	$1.22^{+0.8}_{-0.57}$	$10.05^{+0.07}_{-0.06}$	$7.66^{+1.12}_{-1.44}$	$0.07^{+0.12}_{-0.17}$	$1.8^{+0.42}_{-0.35}$
2006le	low	0.0174	$0.57^{+0.06}_{-0.05}$	$10.25^{+0.03}_{-0.03}$	$1.89^{+0.72}_{-0.51}$	$-1.07^{+0.09}_{-0.09}$	$0.4^{+0.16}_{-0.11}$
2007af	low	0.0055	$0.01^{+0.09}_{-0.0}$	$9.36^{+0.09}_{-0.7}$	$296.92^{+68.29}_{-265.39}$	$-1.06^{+0.8}_{-0.07}$	$6.0^{+0.29}_{-2.04}$
2007le	high	0.0067	$3.34^{+1.56}_{-1.42}$	$9.57^{+0.07}_{-0.1}$	$0.64^{+0.06}_{-0.06}$	$-1.14^{+0.08}_{-0.05}$	$0.87^{+0.12}_{-0.11}$
2007qe	high	0.024	$0.13^{+0.05}_{-0.02}$	$8.13^{+0.06}_{-0.06}$	$0.91^{+0.09}_{-0.09}$	$-1.05^{+0.05}_{-0.08}$	$1.23^{+0.12}_{-0.12}$
2008bf	low	0.0244	$0.95^{+0.06}_{-0.05}$	$10.34^{+0.01}_{-0.02}$	$0.18^{+0.23}_{-0.09}$	$-0.12^{+0.1}_{-0.11}$	$0.44^{+0.11}_{-0.1}$
2008ec	low	0.0163	$0.9^{+0.78}_{-0.39}$	$10.44^{+0.12}_{-0.11}$	$35.13^{+14.03}_{-11.54}$	$0.23^{+0.05}_{-0.08}$	$2.48^{+0.47}_{-0.37}$
2001V	low	0.015	$1.26^{+1.35}_{-0.54}$	$8.99^{+0.14}_{-0.05}$	$0.13^{+0.11}_{-0.05}$	$-1.16^{+0.05}_{-0.03}$	$0.39^{+0.23}_{-0.15}$

Table C.1. continued.

SN Name	Type	$z$	$t_m$	$\log(M_*/M_\odot)$	SFR [ $M_\odot/\text{yr}$ ]	$\log(Z_*/Z_\odot)$	$A_V$ [mag]
2005hk	low	0.013	0.42 <sup>+0.02</sup> <sub>-0.02</sub>	8.53 <sup>+0.02</sup> <sub>-0.02</sub>	0.1 <sup>+0.01</sup> <sub>-0.01</sub>	-1.19 <sup>+0.01</sup> <sub>-0.01</sub>	0.07 <sup>+0.02</sup> <sub>-0.02</sub>
2006ax	low	0.0167	6.11 <sup>+2.74</sup> <sub>-2.21</sub>	9.89 <sup>+0.1</sup> <sub>-0.13</sub>	0.0 <sup>+0.01</sup> <sub>-0.0</sub>	-0.54 <sup>+0.22</sup> <sub>-0.18</sub>	1.16 <sup>+0.35</sup> <sub>-0.41</sub>
2006lf	low	0.0132	0.52 <sup>+0.04</sup> <sub>-0.03</sub>	9.87 <sup>+0.02</sup> <sub>-0.02</sub>	0.94 <sup>+0.26</sup> <sub>-0.2</sub>	-1.18 <sup>+0.02</sup> <sub>-0.01</sub>	0.2 <sup>+0.06</sup> <sub>-0.05</sub>
2007bd	high	0.0257	1.29 <sup>+0.29</sup> <sub>-0.49</sub>	10.09 <sup>+0.05</sup> <sub>-0.04</sub>	0.1 <sup>+0.24</sup> <sub>-0.09</sub>	-1.16 <sup>+0.05</sup> <sub>-0.03</sub>	0.07 <sup>+0.07</sup> <sub>-0.04</sub>
2007ci	low	0.018	8.61 <sup>+1.45</sup> <sub>-1.2</sub>	10.69 <sup>+0.04</sup> <sub>-0.04</sub>	0.01 <sup>+0.01</sup> <sub>-0.01</sub>	-0.36 <sup>+0.03</sup> <sub>-0.06</sub>	0.01 <sup>+0.01</sup> <sub>-0.0</sub>
2005kc	low	0.0151	3.12 <sup>+1.92</sup> <sub>-1.72</sub>	10.64 <sup>+0.17</sup> <sub>-0.16</sub>	12.27 <sup>+8.44</sup> <sub>-7.79</sub>	0.04 <sup>+0.14</sup> <sub>-0.17</sub>	1.73 <sup>+0.46</sup> <sub>-0.52</sub>
2007on	low	0.0065	10.32 <sup>+0.48</sup> <sub>-0.78</sub>	10.83 <sup>+0.02</sup> <sub>-0.03</sub>	0.04 <sup>+0.0</sup> <sub>-0.0</sub>	-0.47 <sup>+0.05</sup> <sub>-0.04</sub>	0.04 <sup>+0.01</sup> <sub>-0.01</sub>
2008gp	low	0.033	0.64 <sup>+0.28</sup> <sub>-0.13</sub>	9.88 <sup>+0.04</sup> <sub>-0.05</sub>	2.61 <sup>+1.12</sup> <sub>-0.75</sub>	0.13 <sup>+0.1</sup> <sub>-0.15</sub>	1.53 <sup>+0.42</sup> <sub>-0.37</sub>
2008hv	low	0.0126	3.47 <sup>+0.87</sup> <sub>-0.62</sub>	10.27 <sup>+0.06</sup> <sub>-0.06</sub>	0.0 <sup>+0.0</sup> <sub>-0.0</sub>	-0.93 <sup>+0.09</sup> <sub>-0.07</sub>	0.02 <sup>+0.02</sup> <sub>-0.01</sub>
2003W	high	0.0201	2.03 <sup>+1.0</sup> <sub>-0.79</sub>	10.29 <sup>+0.11</sup> <sub>-0.11</sub>	10.22 <sup>+3.2</sup> <sub>-2.83</sub>	0.04 <sup>+0.11</sup> <sub>-0.18</sub>	0.99 <sup>+0.28</sup> <sub>-0.18</sub>
2003Y	faint	0.0169	5.58 <sup>+0.94</sup> <sub>-1.2</sub>	10.52 <sup>+0.05</sup> <sub>-0.07</sub>	0.0 <sup>+0.0</sup> <sub>-0.0</sub>	-0.74 <sup>+0.08</sup> <sub>-0.07</sub>	0.05 <sup>+0.04</sup> <sub>-0.03</sub>
2005M	low	0.0246	0.28 <sup>+0.08</sup> <sub>-0.11</sub>	8.84 <sup>+0.1</sup> <sub>-0.13</sub>	2.05 <sup>+1.04</sup> <sub>-0.94</sub>	-1.09 <sup>+0.11</sup> <sub>-0.08</sub>	0.2 <sup>+0.17</sup> <sub>-0.17</sub>
2006X	high	0.0052	0.36 <sup>+0.16</sup> <sub>-0.12</sub>	10.11 <sup>+0.28</sup> <sub>-0.12</sub>	24.81 <sup>+7.75</sup> <sub>-17.63</sub>	0.26 <sup>+0.03</sup> <sub>-0.06</sub>	1.68 <sup>+0.28</sup> <sub>-0.23</sub>
1991bg	faint	0.0034	5.8 <sup>+0.41</sup> <sub>-0.37</sub>	10.75 <sup>+0.02</sup> <sub>-0.02</sub>	0.0 <sup>+0.0</sup> <sub>-0.0</sub>	0.28 <sup>+0.02</sup> <sub>-0.02</sub>	0.02 <sup>+0.02</sup> <sub>-0.01</sub>
1999aa	low	0.0145	5.85 <sup>+0.97</sup> <sub>-1.05</sub>	10.28 <sup>+0.04</sup> <sub>-0.05</sub>	0.73 <sup>+0.08</sup> <sub>-0.07</sub>	-0.92 <sup>+0.09</sup> <sub>-0.07</sub>	0.88 <sup>+0.16</sup> <sub>-0.17</sub>
1998bu	low	0.003	1.87 <sup>+1.43</sup> <sub>-0.47</sub>	10.35 <sup>+0.09</sup> <sub>-0.06</sub>	3.79 <sup>+3.38</sup> <sub>-2.4</sub>	0.1 <sup>+0.13</sup> <sub>-0.11</sub>	3.21 <sup>+0.61</sup> <sub>-0.63</sub>
1998bp	low	0.0104	4.07 <sup>+1.41</sup> <sub>-1.1</sub>	10.19 <sup>+0.08</sup> <sub>-0.09</sub>	0.0 <sup>+0.01</sup> <sub>-0.0</sub>	-0.83 <sup>+0.01</sup> <sub>-0.12</sub>	0.08 <sup>+0.07</sup> <sub>-0.06</sub>
1998aq	low	0.0037	0.42 <sup>+0.02</sup> <sub>-0.02</sub>	10.98 <sup>+0.02</sup> <sub>-0.02</sub>	0.32 <sup>+0.03</sup> <sub>-0.03</sub>	-1.19 <sup>+0.01</sup> <sub>-0.01</sub>	0.99 <sup>+0.1</sup> <sub>-0.14</sub>
1996X	low	0.0069	2.52 <sup>+0.62</sup> <sub>-0.54</sub>	8.34 <sup>+0.07</sup> <sub>-0.07</sub>	0.0 <sup>+0.02</sup> <sub>-0.0</sub>	-0.78 <sup>+0.06</sup> <sub>-0.07</sub>	0.08 <sup>+0.02</sup> <sub>-0.02</sub>
1995D	low	0.0066	8.08 <sup>+1.46</sup> <sub>-1.15</sub>	10.14 <sup>+0.05</sup> <sub>-0.05</sub>	0.0 <sup>+0.0</sup> <sub>-0.0</sub>	-1.01 <sup>+0.06</sup> <sub>-0.07</sub>	0.2 <sup>+0.04</sup> <sub>-0.04</sub>
1994ae	low	0.0043	0.6 <sup>+0.03</sup> <sub>-0.03</sub>	9.03 <sup>+0.01</sup> <sub>-0.01</sub>	0.08 <sup>+0.02</sup> <sub>-0.01</sub>	-1.18 <sup>+0.02</sup> <sub>-0.01</sub>	0.82 <sup>+0.14</sup> <sub>-0.12</sub>
1990N	low	0.0034	2.39 <sup>+0.61</sup> <sub>-0.67</sub>	9.29 <sup>+0.06</sup> <sub>-0.08</sub>	0.08 <sup>+0.01</sup> <sub>-0.02</sub>	-1.17 <sup>+0.03</sup> <sub>-0.02</sub>	0.07 <sup>+0.02</sup> <sub>-0.01</sub>
1986G	low	0.0018	0.76 <sup>+0.01</sup> <sub>-0.01</sub>	10.31 <sup>+0.01</sup> <sub>-0.01</sub>	0.29 <sup>+0.04</sup> <sub>-0.03</sub>	-1.18 <sup>+0.02</sup> <sub>-0.01</sub>	0.91 <sup>+0.08</sup> <sub>-0.16</sub>
2011fe	low	0.0008	0.79 <sup>+0.09</sup> <sub>-0.09</sub>	9.42 <sup>+0.02</sup> <sub>-0.02</sub>	0.33 <sup>+0.06</sup> <sub>-0.06</sub>	0.01 <sup>+0.12</sup> <sub>-0.13</sub>	0.82 <sup>+0.16</sup> <sub>-0.13</sub>
2008q	low	0.008	10.62 <sup>+0.21</sup> <sub>-0.41</sub>	10.77 <sup>+0.01</sup> <sub>-0.02</sub>	0.05 <sup>+0.01</sup> <sub>-0.01</sub>	-0.34 <sup>+0.05</sup> <sub>-0.05</sub>	0.19 <sup>+0.05</sup> <sub>-0.05</sub>
2006D	low	0.0085	0.55 <sup>+0.2</sup> <sub>-0.21</sub>	9.26 <sup>+0.08</sup> <sub>-0.11</sub>	3.69 <sup>+0.34</sup> <sub>-0.29</sub>	-0.91 <sup>+0.21</sup> <sub>-0.16</sub>	2.33 <sup>+0.24</sup> <sub>-0.25</sub>
2005ke	faint	0.0049	1.08 <sup>+0.31</sup> <sub>-0.19</sub>	9.47 <sup>+0.06</sup> <sub>-0.03</sub>	0.05 <sup>+0.04</sup> <sub>-0.03</sub>	-1.17 <sup>+0.05</sup> <sub>-0.02</sub>	0.07 <sup>+0.02</sup> <sub>-0.01</sub>
2003hv	low	0.0056	3.56 <sup>+0.78</sup> <sub>-0.59</sub>	10.21 <sup>+0.05</sup> <sub>-0.06</sub>	0.0 <sup>+0.0</sup> <sub>-0.0</sub>	-1.03 <sup>+0.05</sup> <sub>-0.07</sub>	0.05 <sup>+0.01</sup> <sub>-0.01</sub>
2003du	low	0.0064	0.53 <sup>+0.56</sup> <sub>-0.29</sub>	8.2 <sup>+0.15</sup> <sub>-0.16</sub>	0.33 <sup>+0.18</sup> <sub>-0.13</sub>	-0.79 <sup>+0.2</sup> <sub>-0.2</sub>	1.14 <sup>+0.31</sup> <sub>-0.3</sub>
2002dp	low	0.0116	0.28 <sup>+0.03</sup> <sub>-0.02</sub>	9.62 <sup>+0.04</sup> <sub>-0.05</sub>	4.41 <sup>+0.4</sup> <sub>-0.33</sub>	-1.11 <sup>+0.09</sup> <sub>-0.06</sub>	0.49 <sup>+0.08</sup> <sub>-0.06</sub>
2002cs	high	0.0158	10.52 <sup>+0.34</sup> <sub>-0.75</sub>	10.74 <sup>+0.02</sup> <sub>-0.02</sub>	0.02 <sup>+0.01</sup> <sub>-0.01</sub>	-0.07 <sup>+0.06</sup> <sub>-0.07</sub>	0.11 <sup>+0.06</sup> <sub>-0.05</sub>
2000E	high	0.0048	0.46 <sup>+0.05</sup> <sub>-0.03</sub>	9.68 <sup>+0.02</sup> <sub>-0.03</sub>	1.36 <sup>+0.18</sup> <sub>-0.15</sub>	-1.15 <sup>+0.06</sup> <sub>-0.03</sub>	0.77 <sup>+0.09</sup> <sub>-0.09</sub>
1999by	faint	0.0021	10.63 <sup>+0.17</sup> <sub>-0.33</sub>	9.9 <sup>+0.01</sup> <sub>-0.01</sub>	0.01 <sup>+0.0</sup> <sub>-0.0</sub>	-1.11 <sup>+0.04</sup> <sub>-0.04</sub>	0.08 <sup>+0.01</sup> <sub>-0.01</sub>
1991T	low	0.0058	5.84 <sup>+1.74</sup> <sub>-1.78</sub>	10.92 <sup>+0.05</sup> <sub>-0.07</sub>	2.24 <sup>+1.22</sup> <sub>-0.7</sub>	0.06 <sup>+0.15</sup> <sub>-0.14</sub>	1.02 <sup>+0.65</sup> <sub>-0.4</sub>

**Notes.** The types of each SNe Ia studied in this work (low velocity and high velocity and or faint) the host galaxy redshifts, stellar population ages ( $t_m$ ), stellar masses ( $\log(M_*/M_\odot)$ ), SFRs, stellar metallicities ( $\log(Z_*/Z_\odot)$ ), and total dust extinction ( $A_V$ ). All redshifts are from NED.